UNIVERSITY OF CALIFORNIA,

IRVINE

Experimental investigation of aerodynamic characteristics of a 4-winged flapping mechanism

THESIS

submitted in partial fulfillment of the requirements

for the degree of

MASTER OF SCIENCE

in Mechanical and Aerospace Engineering

by

Mohamed Zakaria

Thesis Committee

Professor Haithem Taha, Chair

Professor Natascha Buswell

Professor Jacqueline Thomas

2021

Acknowledgment

To:

First, to my father and Mother. I do not think I have enough to say about you to. Enough to thank you two for the huge support you gave me. I love you both so much beyond words. You trusted me until the end, even at times when I did not trust myself.

To my sister, the most persistent and supportive person. You will always be my favorite person. I rely on you in heavy days. I love you to the moon and back. I would never be here without you.

To my friends: Rana, Salma, Hoda, Bayoumi, Maher, and Swailm. You guys went with me through thick and thin. You put up with my complaining, my talking, and always tried to make me happy.

To My colleagues: Dipan, Nabil, Kevin, Ming, Cody, Marlon, Laura, Mahmoud, and Asmaa. I learned so much from each person. I am forever grateful.

To Moatasem, man I cannot thank you enough. You spent nights teaching me “how to walk” in the lab. You had so much patience with me. You came at times in the middle of the night just to help me out. You taught me how to do proper work, to the extent of perfection and nothing below that. I do not know what to say except that I will always remember what you did for me until I die. In this small journey, I won a mentor and a friend.

To Professor Taha, you sir changed my life. I know that this can be a bit of an exaggeration for you, but I really mean the word. You made me reconsider the way I comprehend everything in life. You taught me that life is simple. You taught me that one can master anything if persistence and some bravery is present. I called you a lot, talked to you a lot, and I was annoying at times. Yet, you always received my complaints with a smile, and addressed them. You were always there for me even for personal matters. I know that I should have put a lot more effort in this Masters. I recognize that I should have gone more than the stage I am in now, and again you always supported me at the end. Thank you, sir, for everything!

TABLE OF CONTENTS

List of figures

page

Abstract

Experimental Demonstration of different characteristics of 4-winged flapping mechanism

The subject of flapping flight has been studied extensively for more than a century. Flapping flight, throughout the years, has been observed to have different thrust, lift, and moment characteristics that make this phenomenon very efficient when compared to conventional aircraft. This work is a step towards developing a novel flying concept: a quad-flapping drone. An experimental setup was built to measure these different characteristics of a 4-winged flapping mechanism that include lift, drag, pitching moment, and rolling moment. These characteristics made us determine how the clapping effect can be of use to FWMAV (flapping wing micro air vehicles). A second part of this work is the determination of an optimum design point (frequency) in which the mechanism will operate at. This will help in the sizing process of the quad-flapping drone. Lastly, an estimation of the beating angle was put forth by using the hall effect sensor raw data. It was found that the effect of the clapping effect increases with frequency. Also, that the thrust cycle of our FWMAV includes two thrust peaks; one corresponding to the leading-edge vortex, and other is due to clapping. The optimal design point was found by taking the average thrust and power per cycle, nondimensionalizing each term to get the coefficients, and then obtaining $\frac{C_T}{C_P}$ to get the optimal point. This experiment was done for different

areas. It was found that the efficiency increases as the area increases, which is a great result in the sense that higher areas can be of more thrust and the difference in weight would not be great, since the weight of the flapping wing is very small.

Chapter 1

Introduction

Steady analysis has been very sufficient when it comes to conventional aircraft modeling. The simple equations of the lift and drag, without the inclusion of the time, eased things up very much and made the analysis as simple as it can be. Classical Aerodynamics is mainly focused on wings in steady motion, where there is no variation of the wing speed, acceleration, or attitude with time. Flapping mechanisms, however, have a periodic behavior in which there is a continuous change with time. Due to this periodicity, a more descriptive and representative analysis needed to be used; *quasi-steady assumption.* This assumption reduces the time varying problem into a series of static-instantaneous analysis in which at each instant the forces and velocities are measured using the steady equations. This assumption will be the main groundwork by which we will nondimensionalize our results and measurements to obtain the optimum design point in which the 4-winged mechanism, and consequently, the quad-flapping drone will operate.

1.1 Motivation

Nature always has its ways of fascinating us. The intricateness of flapping mechanism has always been appealing in the sense of being very efficient and agile. Flapping mechanism users such as hummingbirds and insects can recover from a perturbation faster than most control systems built by humans. Characteristics such as these can be used into designing flapping micro air vehicles (FMAVs) that have greater agility than conventional quadcopters. Also, the lightness of FMAVs gives it the ability to hover in the air a bigger amount of time when compared to conventional quadcopters. These characteristics, along with the fact that the flapping mechanism is made from paper wings, makes the quad-flapping drone safe and suitable to wide variety of applications.

1.2 Literature review

The literature review consists of two sections: the first section deals with the aerodynamics of the flapping mechanisms in general. The second section talks about the equations of motions of the flapping mechanism. These two subsections will demonstrate in a historic literary way the development of different aspects of the flapping flight field. In the two sections that follow, a detailed introduction to the aerodynamics of flapping wings and its flight dynamics will be given.

1.2.1 Flapping wing Aerodynamics

The whole story of unconventional aerodynamics began in in the 1930s, when Theodorsen [5] devised the theory of aerodynamic instability and flutter.

Theodorsen was the first to solve this problem using analytical analysis without the use of any numerical methods. Theodorsen divided the velocity potentials due to the flow around and aileron into to parts: circulatory flow and non-circulatory flow. Theodorsen solved his problem in the frequency domain. He used the three main principles that are sufficient to result in a velocity field: Kutta condition, no penetration boundary condition, and the conservation of circulation. This along with the unsteady version of Bernoulli's equation enabled him to get the Force and moment on airfoils in pitching and plunging motions. Using conformal mapping, Theodorsen applied the non-penetrating boundary condition in the non-circulatory solution that related the $u\ and\ v$ of the airfoil to the $v_r\ and\ v_\theta$ of the cylinder. After extensive mathematical manipulations and analysis, he calculated the non-circulatory lift as: $l_{NC} = -m_{added}\ a_{\frac{1}{2}}$, where $a_{\frac{1}{2}}$ is the acceleration at the half chord of the airfoil. This term can be thought of as the force by the fluid on the source. As for the circulatory part, Theodorsen applied the Kutta condition as now, and after using conformal mapping to go to the cylinder domain, the vortex will induce velocities on the cylinder as net circulation is present. The output was the integral equation of circulation in which, for the case of simple harmonic motion, and after extensive mathematical manipulation, leads to the ratio of the Hankel functions in which Theodorsen called $C(k)$.

Talking about circulatory lift, Taha and Rezaei in [35] tackled the circulatory lift aspect from a pure dynamical perspective. The authors shoed that the circulatory lift dynamics is different from circulation lift dynamics. They tested the unsteady aerodynamics of a two-dimensional airfoil, where they used the angle of attack as an input and the lift as the output. They found that unlike what is commonly thought regarding that the circulation leads the lift, it is actually the other way around. They found that there is a between the lift

and circulation in the low frequency range and a fractional integrator in the high frequency range. In conclusion, they found that the commonly known fact that circulatory lift is lift due to circulation is not true, it is a completely arbitrary classification that of circulatory, non-circulatory lift.

Besides Theodorsen, the other pioneer in the unsteady field is Wagner [6]. Wagner analyzed the change in circulation around an airfoil that suddenly started from rest. His results showed the time evolution of both the circulation and consequently the lift. These two pioneers hold the ground framework on which the unsteady aerodynamics theory is built upon.

At the first glance, the connection between the contributions of the previous two pioneers and flapping flight may not be obvious, but in the later sections, such connection will become clear. Also as stressed, these two opened the field of non-conventional flying to generations to come.

Fast forwarding few years, in 1956, T. Weis-Fogh and Martin Jensen made a big review on insect flight aerodynamics and performance [7], [8]. The authors made a review on the three theories of the most complexity at the time, [9] [10] [11] [12], to understand more about the aerodynamics of flapping flight. Weis-Fogh and Jensen concluded that [9] model can only give results, such as the drag profile, the average induced drag, and the oscillation drag on large birds and insects that typically have a small wing beat frequency to forward speed ratio *k.* This was mainly since Holst, E. v. & Kuchemann [9] theory was kinematically oversimplified. As for Walker's theory [10], [11], the authors saw that this theory was more complete as it considered the effect of *k* by accommodating for extra wind pressure as *k*

increases. Although, a small refinement of this theory would later be made because for an inclined stroke plane, the induced velocity calculations would differ. Osborne's theory [12] was the most complex of them all as it considered many parameters. Osborne tackled the problem from a theoretical perspective. His main assumption was that the force acting on the wing surface due to arbitrary movement was proportional to the relative wind velocity squared. The force is then resolved into lift and drag, integrated over the wing surface, and then averaged over the total wing beat. Osborne's analysis was mainly concerned with inclined stroke planed flyers and vertical ones. He assumed that all the aerodynamic force comes from the downstroke phase only. This assumption is not applicable to hummingbirds, for instance. In hi numerical results, he found most insects adhere to normal aerodynamic phenomena in which unusual forces such as the inertial forces are not effective. Some of his results had unexpectedly high C_L coefficients, but again he concluded that those results do not mean that there are inertial forces involved partly because the assumptions regarding these bird with high lift coefficients were not right or the analysis accuracy was misleading in some way. Again, all the analysis done here was on forward flight, the limiting case of hovering is still yet to be discussed. This is also one of the reasons why the standard aerodynamics can suffice and gave the above authors satisfactory results.

Furthermore, in their second review paper [2], the authors made a study on how the different stroke parameters can affect the different aerodynamic forces produced by a Desert Locus insect. The insect was suspended from a balance and flew against a wind tunnel. The wind speed was the speed at which the thrust of the locust equals the drag. The lift was measured as the apparent weight reduction. It was found that although the lift varied significantly, stroke parameters such as the stroke angle, the stroke plane angle, and

the time course of the angular movement of the entire wing had a very little to no change at all. The authors found that the lift variation must be explained by a more intricate way than the simple actuator disk.

It was not until 1972 that T. Weis-Fogh made his first breakthrough in the study of flapping flight; the "clap and fling mechanism" [14]. Although Weis-Fogh concluded that even in hovering, the majority of animals including large lamellicorn beetles sphingid moths can still be studied using quasi steady models, some small sized groups especially the ones flying in low Reynolds number such as the true-hoverflies, large dragonflies, and numerous butterflies. On his study in *Encarsia Formosa* (a species of chalcidoid wasp), in a Reynolds number of (10-20) the insect produced a very high lift coefficient that cannot be attained using normal aerodynamics. He then concluded that there must be an unconventional aerodynamics mechanism that helps the *Encarsia* reach this high lift coefficient. Weis divided this novel phenomenon relating to the movement of the *Encarsia* wings into 3 phases: the *clap,* the *fling,* and the *flip.* The *clap* is the part in which the wings are closely bound together in the upstroke, the *fling* in which the insect's wings start descending in its plane in the downstroke phase, and the *flip* in which the wings supinate at the beginning of the upstroke. Weis described the *fling* part as the part responsible for setting up the appropriate amount of circulation around the wing. This description proved right in the findings of the experiments done by T. Maxworthy in 1979 [15].

In 1984, Ellington, C. P. produced the most complete study on flapping wings, up to date, in which he included nearly all engineering and biological parameters that relates to bird and insect flight [1], [2], [3], [4], [17], [18]. He wanted to address dome of the points studied by

T. Weis-Fogh in his papers [7], [8], [13], [14], and specifically the validity of the quasi – steady assumption.

In his first paper [1], Ellington started by answering the question in why flutter analysis, for instance, cannot be used to study flapping aerodynamics. He reasoned that flutter analysis is restricted to linearizations that depend on small amplitude oscillations, which is not applicable to neither insects nor birds. Drone-flies, for example, can reach a flapping angle of 106 degrees. The author started by introducing the blade element theory, which is the one used to treat aerodynamics of flapping flight by previous pioneers such as Osborne [12]. The basic unit of analysis is the wing element, infinitesimal wing element dr, in the spanwise direction. The aerodynamic force F' is then resolved into a horizontal component and a vertical component. More accurately, the component normal to the flow velocity, lift, and the component parallel to the flow velocity, drag. The lift and drag on this wing section with a spanwise width dr:

$$L' = \frac{1}{2}\rho c U_r^2 C_L \qquad (1)$$

$$D' = \frac{1}{2}\rho c U_r^2 C_{D,pro} \qquad (2)$$

Where pro here stands for profile drag. Since we are talking about the quasi-steady assumption, the coefficients C_L & $C_{D,pro}$ are functions of the Reynolds number and the relative angle of attack at a given time instant. For hovering flight, the drag equation should be equated to zero and the lift equation to the weight of the animal.

The U_r is the vector sum of the velocity of the flapping U and the induced bound and wake vortices. The blade element theory ignores the existence of the wake and bound velocity vortices, and the induced velocity is estimated using the Rankine-Froude axial momentum theory of propellers. Another drawback of this method is the need of complete kinematic data in order to solve in a successive step wise solution using equations (1) and (2): the longitudinal wing axis motion, angle of attack, and the section profile all must be known as a function of time and radial positions. The coefficients $C_L \; an \; C_{D,pro}$ to be known from experimental measurements. This method, though, becomes fallible as we get close to hovering state, where considerations of bound vortices and wake induced velocities become significant. In the coming chapter, we will talk about the aerodynamic of flapping flight of hovering insects in detail following the groundbreaking work of Dickinson and Sane [16]. Moving on, Osborne [12] introduced a new way of analysis that solves for the mean values of the coefficients, $\overline{C_L} \; and \; \overline{C_{D,pro}}$, satisfying the net balance force. This method greatly simplifies calculations since the measurement of the angle of attack in each profile section is extremely difficult and taking the force coefficients as constant will waive the need for such measurement. Ellington in this series of study chose this mean lift coefficient method in all the hovering analyses to test the quasi – steady assumption. He tested it theoretically by proof – of contradiction: the mean forces are calculated according to quasi – steady assumptions. If these calculated forces do not satisfy the net force of the flying animal, then the assumption fails. If it does satisfy, then this assumption cannot be discounted.

Ellington then went on to dividing all the animals studied into three functional groups, for which the mean force analysis using the quasi – steady assumption can be applied with some approximation:

- Horizontal stroke plane group
- Inclined Stroke plane group
- Vertical Stroke plane group

During a cycle, animals beat through an approximate *stroke plane.* It is measured with respect to an the horizontal by an angle β. Each of the groups mentioned has its unique characteristics due to its stroke plane classification. This will impact the way in which the calculation is conducted and, as will be discussed, how the relative velocity measurements will differ from one group to another.

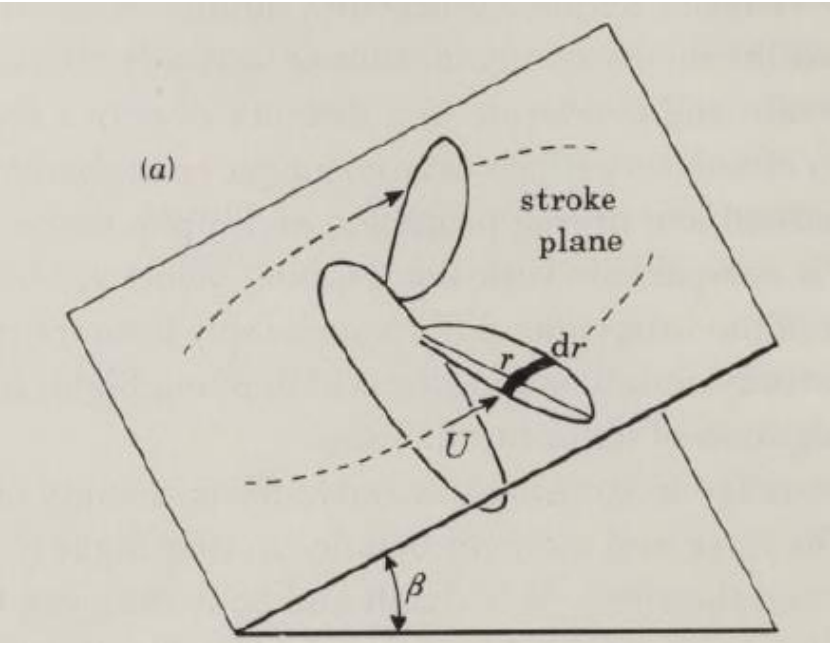

Fig.1 Taken from reference 1, schematic of the stroke plane measurement.

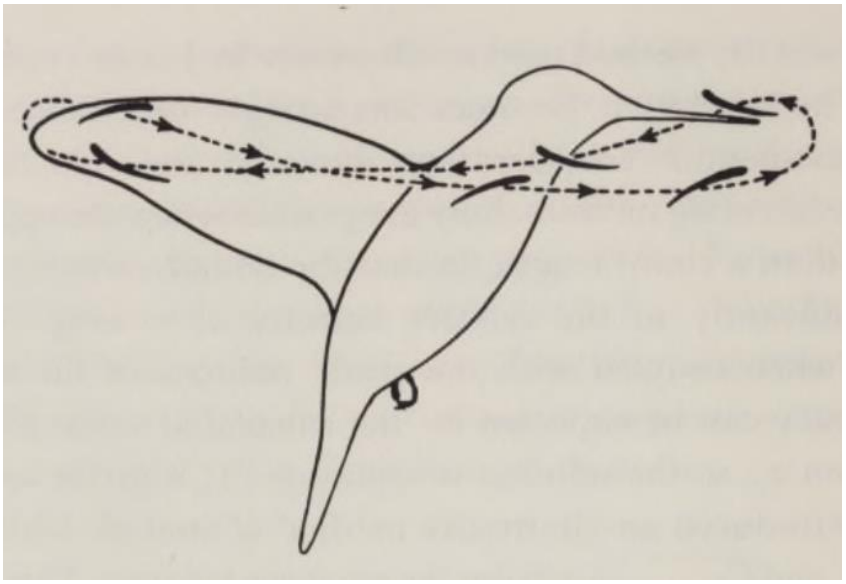

Fig. 2 Taken from reference [1], wingtip path of a hummingbird.

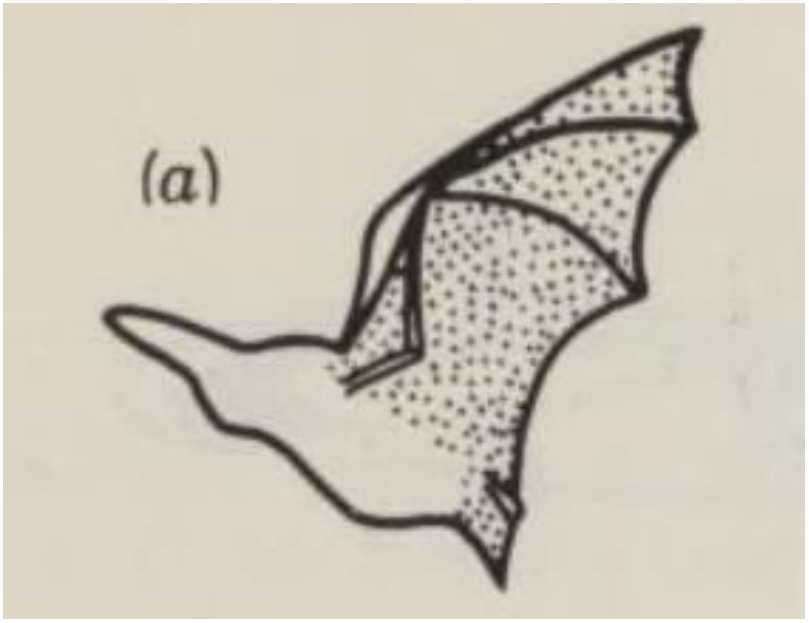

Fig, 3, taken from reference [1],
wingbeat of the long-eared bat.

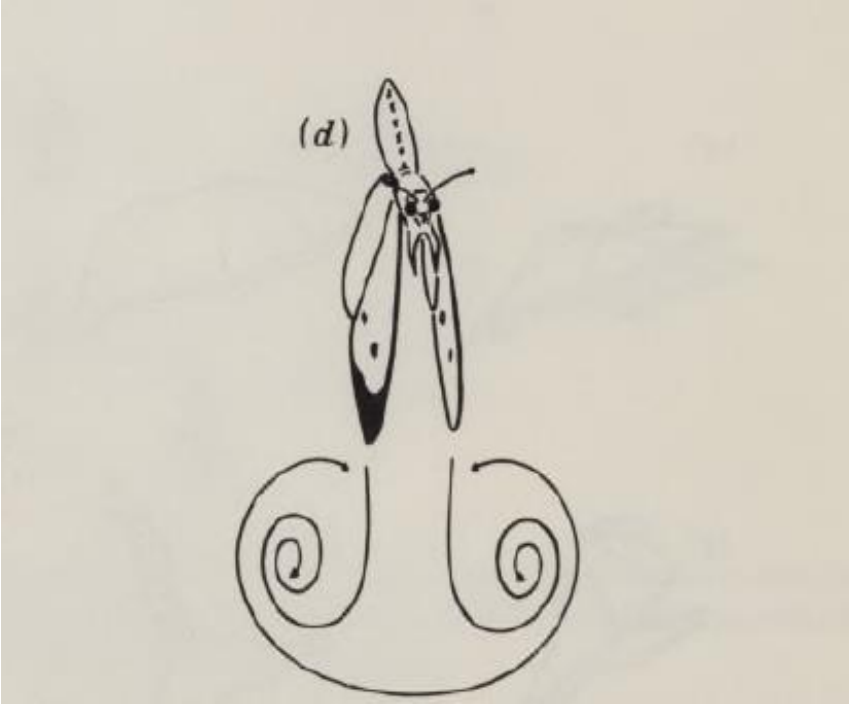

Fig, 4, taken from reference [1], downstroke of a *Pieiris brassicae*.

Starting with the horizontal stroke plane group, it is the most observed hovering animals between the three groups. This group is also characterized by a large angle of attack in both the upstroke and the downstroke. According to Ellington in [20], the wake induced velocity for this group is insignificant with respect to the flapping velocity, which makes the use of the horizontal flapping velocity U_r appropriate in this case. This assumption allows an easy calculation of the mean lift coefficient by balancing equation (1) with the body mass and integrating over the span. An example of this family is the hummingbird in figure (1).

The wingbeat of the long-eared bat in figure (2) is an example of the inclined stroke plane flyer. The flyers of this family can hover with a stroke plane up to β equal 60 degrees. The birds and bats in this family flex their wings during upstroke and the wings come to near

90 degrees. This causes all the force in the upstroke to be directed towards the horizontal, and very negligible lift. This indicates that the downstroke is the main source for weight support.

Unlike the horizontal stroke plane family, the relative velocity U_r cannot be estimated as the flapping velocity effect alone. Due to the inclination of the stroke plane, the induced velocity will affect the value of U_r.

As for the vertical stroke plane family, like the butterfly shown in figure (3), the wings clap together at the ends of downstroke, and then "fling" open. This is one of the animals that use the "clap and fling" mechanism that was discovered by Weis – Fogh [14] and that was talked about previously in this review. Similar to the inclined stroke plane family, all the weight support force comes from the downstroke part, leaving little force generated in the upstroke. The thrust component, though, is augmented in both the strokes. The clap and fling mechanism here is obvious, leaving a little room for any doubt about using the quasi-steady analysis.

Ellington concluded that for animals in the inclined or vertical stroke plane family, the quasi – steady analysis treatment is insufficient as these groups rely mainly on unconventional unsteady flight mechanisms. For the horizontal stroke plane family, the proof was not conclusive for most animals as the $\overline{C_L}$ values are close to those of $C_{L,max}$ (maximum steady – state lift coefficient). The only obvious exception was the insect *Encarsia,* which is the same insect that Weis – Fogh experimented on and discovered the "clap and fling" mechanism in 1973 [14].

In his second paper [2], Ellington discusses the morphological parameters of the birds' and insects' wings. Ellington divided theses parameters into two groups: gross parameters and shape parameters. The gross parameters provide a crude description of the animal's morphology: the body's mass, body length, wing length, and wing area. Another very important parameter that was first invoked upon by Theodorsen in his paper [5], is the virtual mass or added mass. This is the air mass that is accelerated under the wing at the upstroke and the downstroke. This virtual mass approximately equals the air mass contained in an imaginary cylinder, with the chord as its diameter. Experiments showed that the value of the virtual mass ranges from 0.3 to 1.3 times the actual wing mass, which is significant.

Non-dimensional radii derived from the non-dimensional moments of distributions are the shape parameters. These parameters include the first radius of wing mass which gives the center of mass position of the wing, and the second radius of wing mass or simply the radius of Gyration. Lastly, Ellington found relations between the radii of mass, wing area, and virtual. He concluded from these relations that flying animals follow some form of "law of shape", he called it, irrespective of their biological differences.

In Ellington's third paper in this series [3], he demonstrated how he filmed each of the wide range of insects and birds. Insects were filmed at a rate of 5000 frames per second to be able to extract the wing and body motion accurately. Ellington used a projection technique that transforms the insect body coordinate system to the camera's, and vice versa. This transformation allowed Ellington to output all the kinematic details of the longitudinal wing and body axes from the films.

Ellington observed that a lot of the sequences were devoid of complete hovering. Most animals would fly around the test chamber, and in only few moments would there be "hovering". This made him observe that there was a tilt in the stroke plane angle β prior to the forward acceleration, and this makes sense in that the flying animal is directing its dominant force to move and maneuver in specific directions.

Another nice observation is that the body angle itself oscillates with the upstroke and the downstroke. Maximum oscillations found were around $\pm$ 3 degrees for the Ladybird. Maximum and minimum body angles were at the end of the strokes, where the biggest nose-down pitch moments at the upstroke (dorsal) and the biggest nose-up pitch moments at the downstroke (ventral). Ellington reasoned that the pitching moment is caused by three forces:

- Lift force acting on the wing length.
- Drag force acting on the moment arm between the wing base and c_g.
- The virtual mass (inertial wing forces)

We will be talking in detail about the body oscillations and how such oscillations stabilize a bird in hovering, a groundbreaking work by Haithem Taha [21].

In his 4th paper of this review, Ellington went on and explicitly reviewed the unsteady mechanisms in the hovering state of flying animals. Ellington first made a small introduction about the conventional lift mechanism and how the famous $2\pi\alpha$ result is found. He also called this result a circulatory lift, since it originated from how the circulation Γ is calculated.

Fast forwarding into 1999, Dickinson and Sane made their groundbreaking on the basis of insect flight [16]. They made an experiment do discover the underlying physics on to how the birds can maintain their weight in hover. They attributed the bird flight into three different phenomena: Delayed stall, Rotational circulation, and Wake capture. A detailed explanation will be provided in chapter 2 of this thesis talking about this paper.

In 2001, Dickinson went further as to assess the feasibility of the used quasi-steady model in the field [28]. He found that the quasi-steady modeling overestimates the delayed stall phenomenon at some moments and underestimates the rotational circulation. He made an edit to the model in which he measured the rotational force coefficient using a series of experiments and included it in the total force term. Details of this paper are also found in chapter two of the thesis.

As just has been mentioned, the quasi-steady modeling still does not capture the full physics of the aerodynamics. This motivated Taha and Hajj in [23] to approach the aerodynamics modeling problem of flapping wings from a complete unsteady perspective. The idea was that Taha used the Duhamel superposition principle to capture non-conventional lift mechanisms such as big leading edge vortex formulation which is the underlying cause of the delayed stall mechanism. The results were confirmed with CFD analysis by Sun & Du in [24].

Since lift production and the formation of vortices are basically viscous processes, this fact motivated Taha and Rezaei in [36] to develop viscous model that is appropriate enough for insect flights at low Re. This is the first model of its kind. The authors used the triple deck boundary layer theory, which is a theory that models the aerodynamics going through the

transition phase from zero slip on the trailing edge to zero stress on the wake. The main modification the authors did to the thin airfoil theory is the introduction of a singularity term in the pressure distribution that corresponds to the trailing edge. Using this developed model, they went on and extended Theodorsen's lift frequency response to include viscous effects. They found that as Re decreases, amplitude of the lift transfer function increases. Lastly, the model showed that the viscosity induces a lift lag that is not captured by Theodorsen's model. More on this matter can be found in [37] and [38] written by Taha.

1.2.2 Longitudinal Dynamics

In 2014, Taha made a great work in coupling between dynamics and longitudinal dynamics of a 2-winged flapping animal [34]. He started the analysis with rigid body longitudinal dynamics and incorporated with it a quasi-steady model. He then derived the stability derivatives for with the flapping angular velocity equals zero. Taha then went on and assessed the stability of this nonlinear time periodic system by using averaging theorem. The author went on to obtain the stability derivatives using complex step finite difference. He found that this technique greatly matches the results of those by Sun in [29]. Although the model lacks unsteadiness, it gives a good estimate for the cycle average stability derivatives.

Does averaging really capture the whole dynamics? In their work in [39], Taha and Hassan assessed the feasibility of the averaging dynamics from a geometric control's perspective. They found that averaging theorem is not capable of capturing all the dynamics because there exists an induced mechanism in the insects, vibrational stabilization, that is due to

high frequency periodic flapping that is ignored in the averaging model. This was further stressed upon and showed by Taha, Tahmasian, and Woolsey in their work for the need of higher order averaging in [40].

As mentioned in the preceding paragraph, the vibrational stabilization is a mechanism in which the insect stabilizes itself in midair at hover by making its wings oscillate at very high frequencies. This was found first experimentally by Taha, Kiani, and Navarro in [41]. They setup at a two degree of freedom setup in which a model bird is able to move about a pendulum and pitch around its own axis. They found that at high frequencies, the bird stabilizes itself back to its original position following any perturbation, even huge ones. This was proven on a real hawkmoth and mathematically modeled using chronological calculus that there is a new term in the pitch dynamics model that accounts for this stabilizing motion. This was found by Taha, Kiani, Hedricks, and Greeter in their groundbreaking work in [11].

Chapter 2

Flapping wing Aerodynamics

In this chapter, extensive explanation of the flapping wing aerodynamics will be given. The first section will be concerned with the groundbreaking work of Dickinson, Lehmann, and Sane on the basis of insect flight and the phenomenon of "wake capture" [16]. This paper explains how insect fly and explores and explains the fundamental causes of why the birds and most insects can have lift forces up to twice their weight. The second section will focus on pronation and supination; their meaning and how they affect the bird flight performance and lift and drag. The third section will be on quasi – steady analysis and some experimental work on this assumption that proves that it suffices for flapping wing analysis. Final section will be on the stroke plane classification. All birds and insects are categorized into 3 classes: Horizontal stoke plane fliers, inclined stroke plane fliers, and vertical stroke plane fliers. Each class has its own characteristics when it comes to aerodynamic analysis.

2.1 Basis of insect flight

Dickinson is considered one of the pioneers of the flapping wing area, his paper about the basis of insect flight opened a new dimension in flapping wing research, and more importantly, made us understand more about the flapping mechanism.

Dickinson attributed the insect performance to three different yet interactive mechanisms:

- Delayed stall
- Rotational circulation
- Wake capture

His motivation for proposing such theory came from the fact that when putting insects inside a wind tunnel and tested over a range of velocities that they encounter, the C_L was found to be a lot smaller than required for the insects to sustain flight. As mentioned earlier by Weis-Fogh in [14], the *clap* and *fling* mechanism is substantial to many flapping fliers, however, it was argued by Dickinson based on Marden work in [19] that not all insects use this mechanism. More studies using a hawkmoth dynamically scaled model suggested that "delayed stall" might be the cause that birds, and insects have such high C_L, they are not sufficient to explain why some insects can have lift values that can exceed twice their body weight. As mentioned earlier, "delayed stall" is a phenomenon in which a leading-edge separation bubble forms at high angles of attack by the generating of circulatory forces that enhances the lift status of the bird or insect compared to those measured in steady state conditions. In this paper, Dickinson answered the questions of the basis of insect flight by

setting up an experiment in which he can measure the forces off a dynamically scaled model of the fruit fly, *Drosophila melanogaster.*

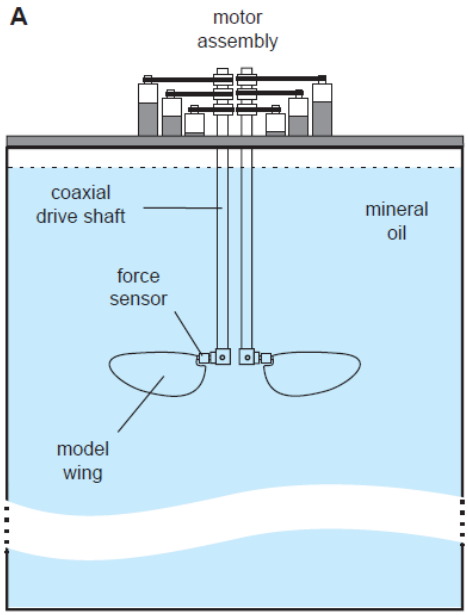

Fig. 5, taken from reference [16], robotic apparatus used for force measurement.

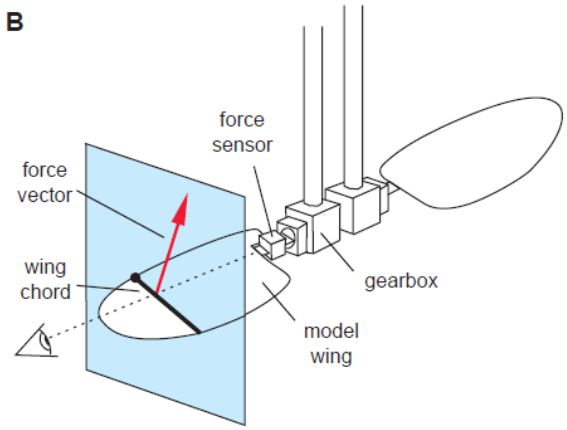

Fig. 6, taken from reference [16], close up view of the measuring fly.

The dimensions of the tank are 1m by 1m by 2m. The tank is filled with mineral oil with a density of $0.88(10^3)\ kgm^{-3}$ and kinematic viscosity of 115 cSt. These parameters were chosen to be able to match the *Re* of the *Drosophila*. The results were taken at stroke amplitude of 160 degrees, frequency of 145 mHz, and midstroke angle of attack at 40 degrees upstroke and 40 degrees downstroke. The average inclination of the wing was 10.3 degrees with respect to the vertical. In the experiment, Dickinson applied three different configurations that he used for comparison to determine which the physics of flapping and in which one is the rotational affects less subtle:

- Advanced wing rotation: in which the model starts turning before reaching the end of the stroke.
- Symmetric wing rotation: in which the model wing starts rotating at the end of one stroke and spans the time until the beginning of another.
- Delayed wing rotation: in which the model wing rotates after beginning the new stroke.

The following schematics show the definitions mentioned applied to the upstroke and the downstroke:

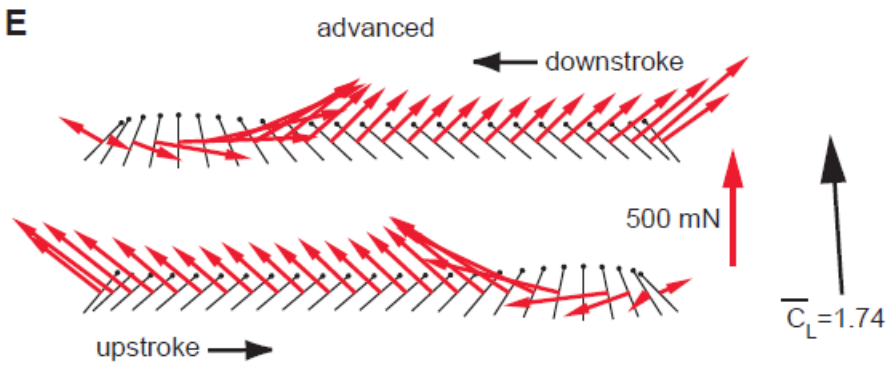

Fig. 7, taken from reference [16], advanced stroke pattern.

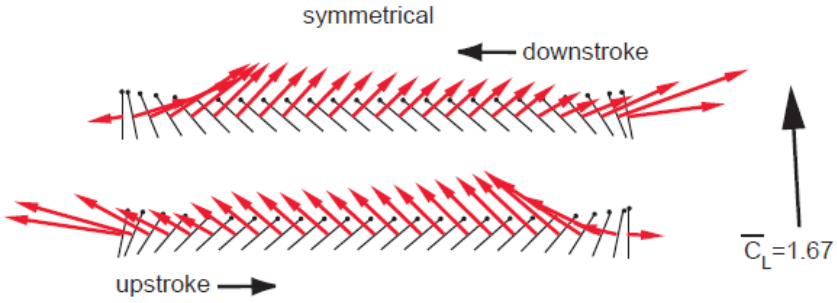

Fig. 8, taken from reference [16], symmetric stroke pattern.

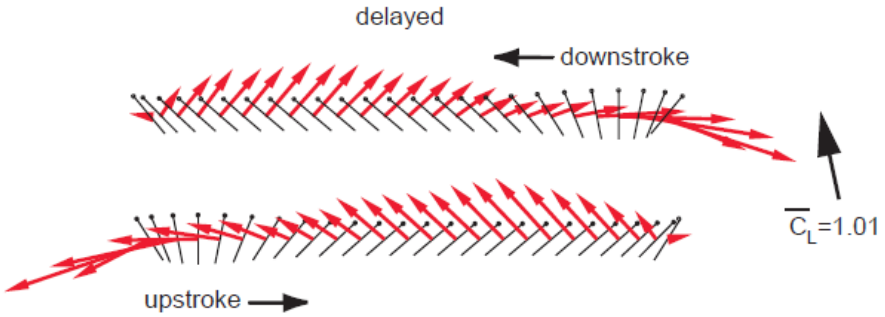

Fig. 9, taken from reference [16], delayed stroke pattern.

Dickinson started by testing whether the translational effect of delayed stall plays the role of the lift augmentation. He first measured the total force given the parameters mentioned, and then to isolate the translational component, he moved the wing 180 degrees at a fixed angle of attack. As shown in figure (),

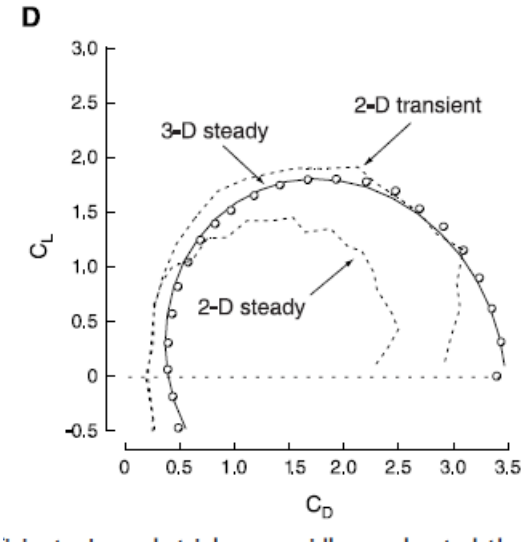

Fig. 10, taken from reference [16], Polar representation of translational force coefficients and comparison to 2D steady and 2D transient.

the 3D steady component (experimental data is manifested in the dots) are below the 2D transient component, and above the 2D steady. This is mainly because that in 2D flow, unstable vortices named “von Karman street” arise, whereas in 3D flow the leading-edge vortex was stable throughout the flight. Moreover, the $C_{L\alpha}$ and $C_{D\alpha}$ curves were found to be nicely fitted by equations (3) and (4):

- $C_L = 0.225 + 1.58\sin(2.13\alpha - 7.2)$ (3)

- $C_D = 1.92 - 1.55\cos(2.04\alpha - 9.82)$ (4)

The results, as shown in figures (11), (12), and (13) suggested that

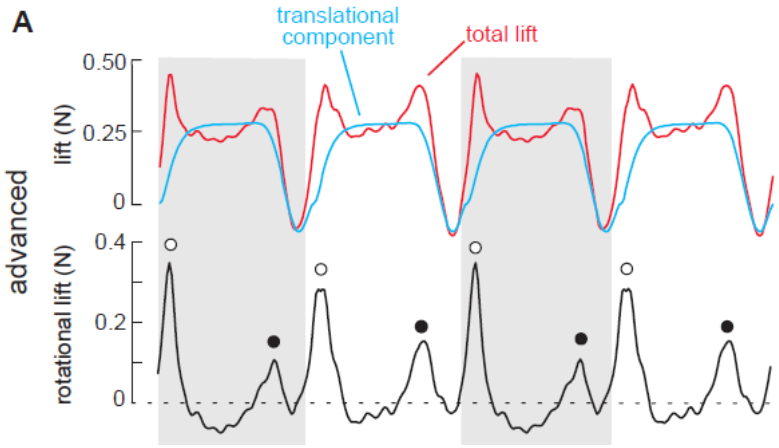

Fig. 11, taken from reference [16], results of total forces, measured translational, and obtained rotational forces in the advanced stroke pattern.

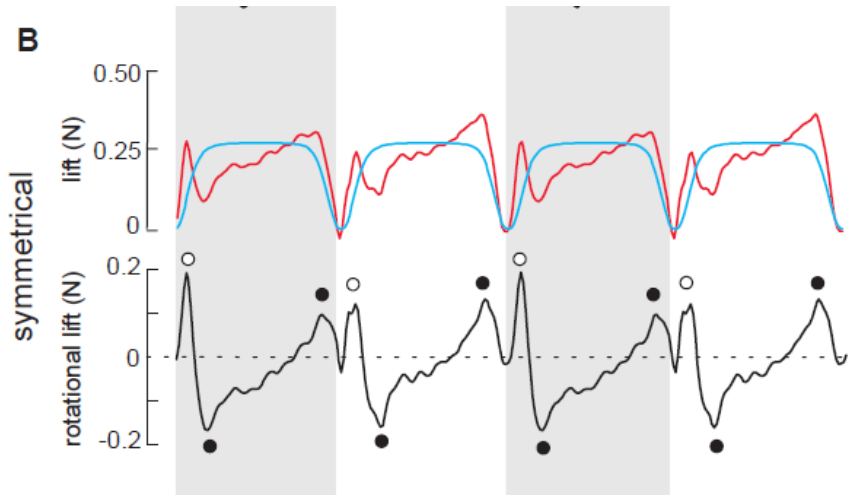

Fig. 12, taken from reference [16], results of total forces, measured translational, and obtained rotational forces in the symmetric stroke pattern.

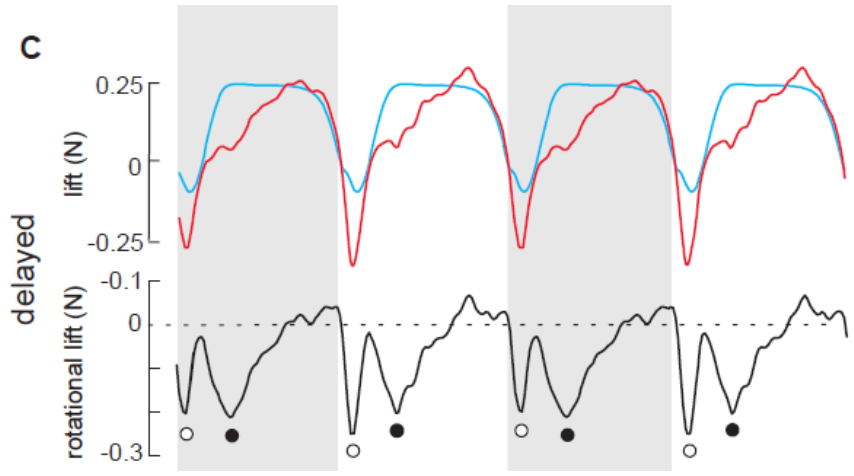

Fig. 13, taken from reference [16], results of total forces, measured translational, and obtained rotational forces in the delayed stroke pattern.

these two force peaks coming from the rotational forces might represent a new aerodynamic mechanism. The rotational forces were obtained from subtracting the already calculated translational forces from the total lift over the cycle. The rotational forces then outputted two peaks as shown in the figure.

Dickinson suggested that these peaks are the result of the wing's own rotation as it changes direction at the end of each stroke. But one important note is that for the wing to accommodate for the coming stroke, it must change direction early (advanced wing rotation) in order not to lose energy and force as was demonstrated in figure (7). Early flip for the wings means the relative angle of attack that is meeting the flow increases, and thereby increasing the lift. If the wing flips late (delayed wing rotation), then at the coming stroke that means the relative angle of attack that is meeting the flow decreasing, and the leading edge meeting the flow is rotating forward with respect to translation, and this will create the downward force. For the symmetric wing rotation, the wing will first generate

lift, then a downward force and both will cancel each other. Dickinson concluded in this part that the bird can optimize the timing of its wing flip in order to maximize the force.

The rotational circulation can explain the stroke reversal forces but cannot explain the large transient peaks after the wing immediately flips going to the beginning of the next stroke, as shown in figure (14) (the transient peaks are the whit dots).

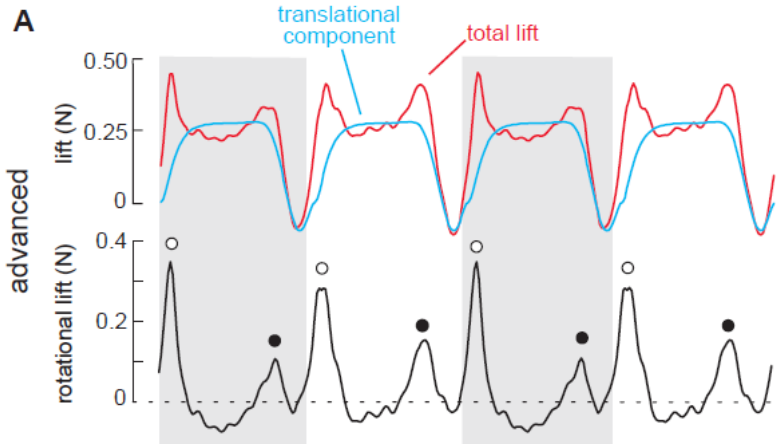

Fig. 14, taken from reference [16], revisiting of Fig. 11 for the explaining of wake capture.

These peaks are in all the configurations; advanced, symmetrical, and delayed wing rotations. The difference between these peaks and the rotational peaks defined before is that the timing of these peaks is independent from the wing rotation configuration. It happens nearly at the same time during the cycle in the three configurations. One explanation, Dickinson proposed, that enables this transient peak is the mechanism of wake capture. Dickinson defined the wake capture as the process in which the wing reuses the shed vorticity of the previous stroke. In order to test this hypothesis, Dickinson tested whether there is an effect from the previous stroke on each cycle by starting the wing and

ending its movement at the end of the cycle. If the hypothesis is true, the wing should generate the force at the end of the half stroke even after stopping the wing motion. His predictions came true, as shown in figure (15).

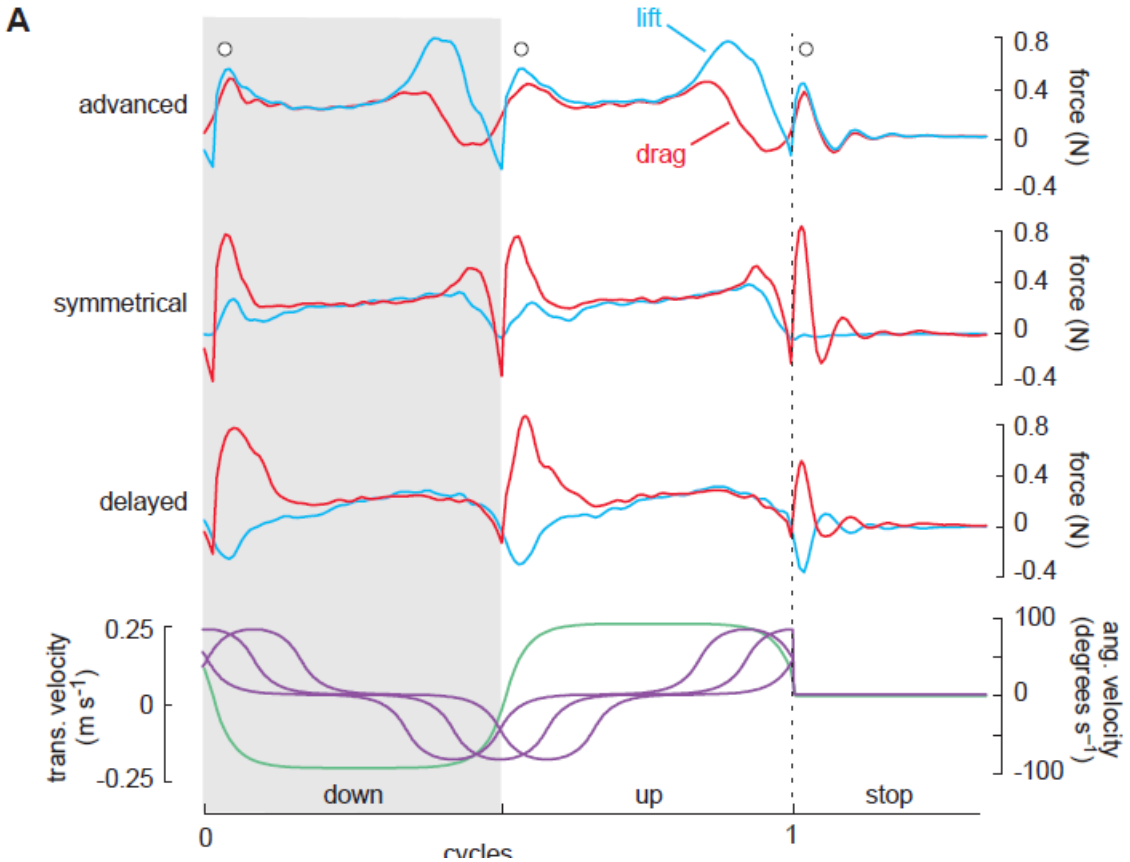

Fig. 15, taken from reference [16], evidence of the wake capture mechanism after the wing comes to a halt.

Again, the timing of the wing rotation makes a significant impact in the magnitude and direction of the force peak. An advanced wing rotation wing rotation will make the wing intercept its own wake, generating a positive lift peak. A delayed wing rotation means the wing intercepts the flow at an angle that hinders the lift, or more accurately produces negative lift. A symmetric wing rotation, the wing has 90 degrees at exactly half of the stroke reversal, and thereby produces no additional lift if stopped at the end of the stroke.

In summary, the author has shown that bird flight cannot be caused by translational forces alone, even if the force is an unconventional translational mechanism such as delayed stall. Rather, the flapping aerodynamics are caused of three phenomena: delayed stall, rotational circulation, and wake capture. The latter two work together in harmony in the pronation and supination phases during stroke reversals.

2.2 Quasi Steady Modeling

In this section, we will be summarizing Dickinson and Sane work they did in editing the known quasi steady model they devised in [28] and adding the rotational effect to it. The authors used the same model they used in [16] (this is the same paper that was summarized in the last section, 2.1):

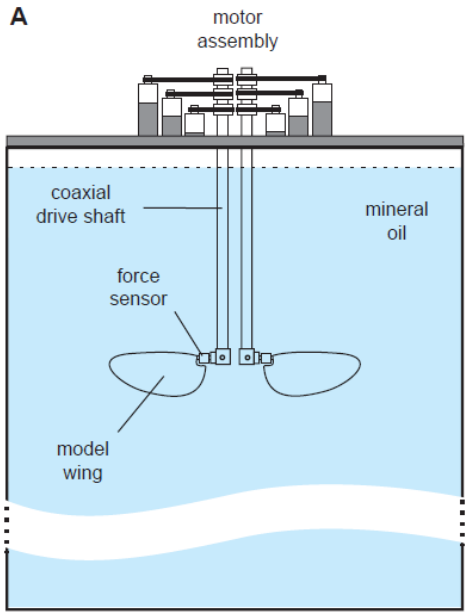

Fig. 16, taken from reference [16], robotic apparatus used for force measurement.

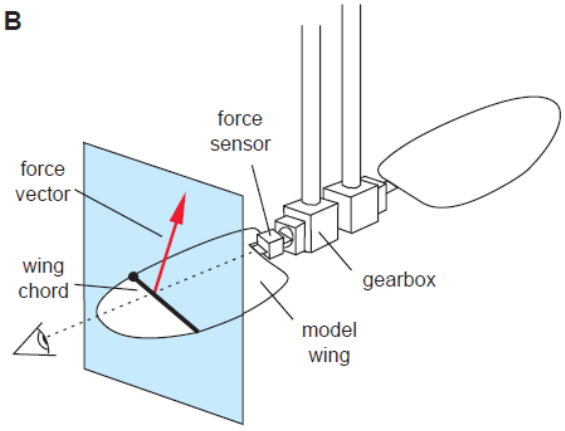

Fig. 17, taken from reference [16], close up view of the measuring fly.

All experiments were done on a Reynolds number of 115, calculated as [4]. The experiment was done over a range of angular velocities: 0 to 1.5 $rad\ s^{-1}$ by increments of 0.085 $rad\ s^{-1}$. The angular velocity was expressed in a non-dimensional form as:

$$- \quad \widehat{\omega} = \frac{\omega \overline{c}}{U_t} \qquad (5)$$

where ω is the absolute angular velocity, $\overline{c}$ is the mean chord length, and U_t is the tip velocity. The experiment was also done over a range of non-dimensional axis of rotation ($\hat{x}_o$) from 0 to 0.66, 0 indicating the leading edge and 1 the trailing edge. Values higher than 0.66 threatened to damage the sensor on the wing due to large moments.

The total force on the wing is:

$$- \quad F_{inst} = F_a + F_{trans} + F_{rot} + F_{wc} \qquad (6)$$

where F_{inst} is the instantaneous force on the wing, F_a is the inertial force due to added mass, F_{rot} is the force due to rotation, and F_{wc} is the force due to wake capture.

If we are to neglect the wake capture effect and inertial added mass, we can isolate our rotational force component:

$$- \quad F_{rot} = F_{inst} - F_{trans} \qquad (7)$$

The F_{inst} is the force measured from the sensor. F_{trans} was estimated using the following equation:

$$- \quad F_{trans} = \frac{\rho S U_t^2 \hat{r}_2^2(S)}{2} \left(C_{Lt}^2(\alpha) + C_{Dt}^2(\alpha)\right)^{\frac{1}{2}} \qquad (8)$$

where S is the projected surface area of the wing and $\hat{r}_2^2(S)$ is the non-dimensional second moment of area according to [4].

Since the rotational forces will be measured form the experiment, we can call F_{rot} to be $F_{rot,exp}$. The non-dimensional coefficient of the rotational force can be calculated as:

$$- \quad C_{rot,exp} = \frac{F_{rot,exp}}{\rho U_t \omega \overline{c^2} R \int_0^1 \hat{r}\hat{c}^2(\hat{r})d\hat{r}} \qquad (9)$$

The results shown in figures (19), (20), (21):

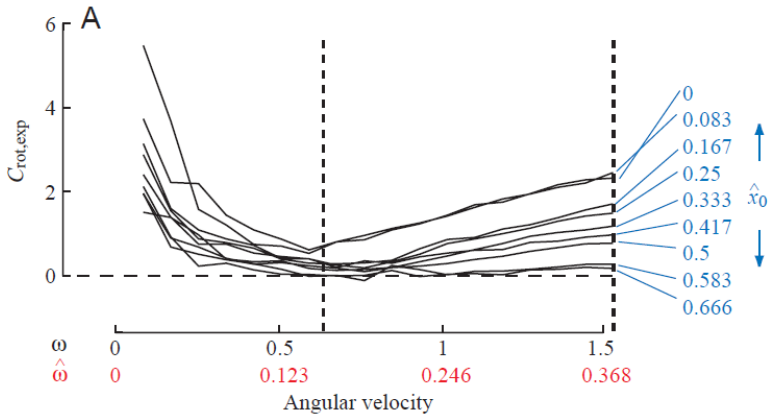

Fig. 18, taken from reference [28], rotational coefficient versus angular velocity for each axis of rotation.

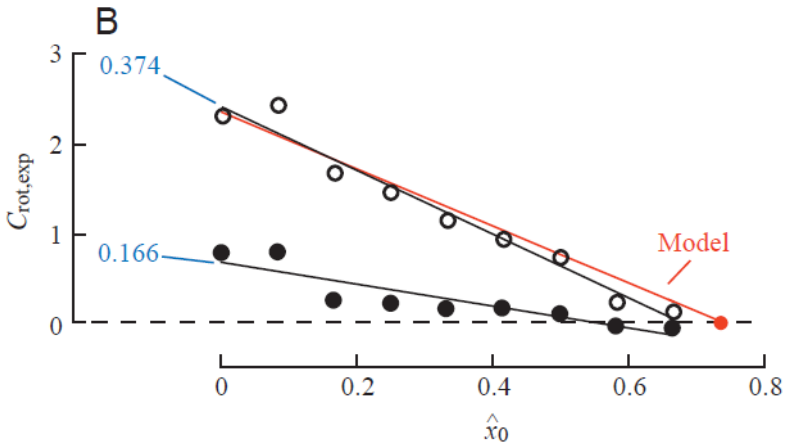

Fig. 19, taken from reference [28], rotational coefficient versus axis of rotation.

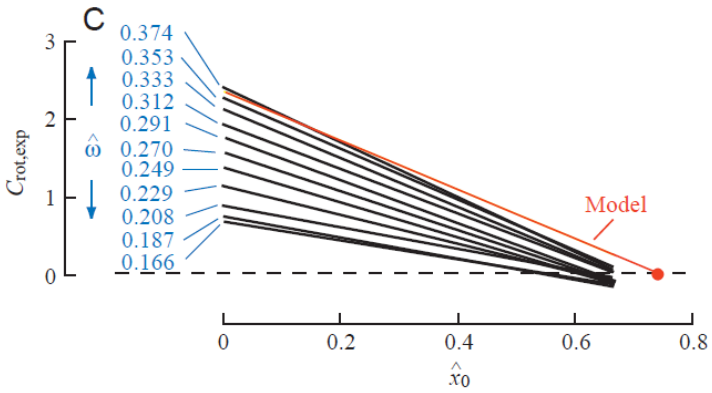

Fig. 20, taken from reference [28], representative values of angular velocities plotted together with the quasi-steady prediction.

that there is a strong dependence on the magnitude of ω, unlike the quasi-steady treatment derived by Theodorsen in [5] (see also [21]). The authors chose $C_{rot,exp} = 1.55$. This was based on the highest angular velocity $\hat{\omega} = 0.374$ and $\hat{x}_o = 0.25$. The authors could not go higher than this regarding the non-dimensional rotational axis due to mechanical constraints.

As shown in the validation results in figure (22),

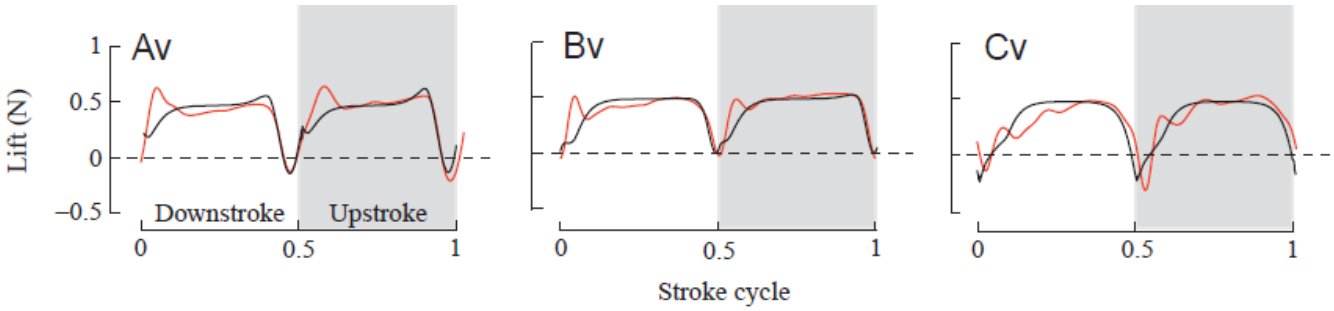

Fig. 21, taken from reference [28], validation of the edited quasi steady model with the three different kinematic patterns: advanced, symmetric, delayed.

the revised model (black) nicely estimates the end of stroke rotational component and translational component but falls short in estimating the wake capture mechanism.

2.3 Unsteady Modeling

In order to account for the full leading edge vortex dynamics, Taha at [23] proposed a complete unsteady model. The author compared the model to CFD [24] and found the results matching and the physics present.

The author makes use of the static lift curve to determine the unsteady lift for an arbitrary wing motion. A unique feature of this work is that instead of using the angle of attack or airfoil speed as the unput, the author uses the quasi-steady circulation as the forcing input. This enables the model to predict the temporal lift build up coming from the stabilized leading-edge vortex, including the lag and phase shifts of unsteady flows. The basic principle in this model is the Duhamel superposition principle.

The first step in incorporating the unsteadiness is the basis of unsteady aerodynamics: the Wagner effect [6]. We can write the unsteady lift in terms of the static lift and the Wagner functions as:

$$- \quad l(s) = l_s W(s) \qquad (6)$$

where l_s is the static lift and $W(s)$ is the Wagner function. The non-dimensional parameter s is defined as

$$- \quad s = \frac{2}{c}\int_0^t U(\tau)d\tau \qquad (7)$$

for varying stream $U(\tau)$. Duhamel superposition principle enables the author to write the circulatory lift as a superposition of indicial response (known) and time-variation of the input variable as:

$$- \quad l(s) = \pi\rho U^2 c(\alpha(0)W(s) + \int_0^s \frac{d\alpha(\sigma)}{d\sigma} W d\sigma) \qquad (8)$$

$W(s)$ can be used as an indicial response to aerodynamic inputs, as done by Van der Wall and Leishman [25]. For a relatively high angle of attack, like the one used by birds and insects, a more exact form of normal velocity is used $w = Usin(\alpha)$:

$$- \quad l(s) = \pi\rho U(s) c(U(0)\sin\alpha(0)W(s) + \int_0^s \frac{dU(\sigma)\sin\alpha(\sigma)}{d\sigma} W d\sigma) \qquad (9)$$

The main problem in the equation mentioned above, and in the classical unsteady approach in general, is that it cannot account for lift mechanisms, such as that coming from the leading-edge vortex forming. As can be seen from above equations, there is a dependence of the lift on $\alpha, U\alpha, and\ Usin\alpha$. This dependence enabled the author to generalize the above equation to using the circulation as an input, knowing that the lift is linearly dependent on circulation in a potential flow. The above equation can be written as:

$$- \quad l(s) = \rho U(s)(\Gamma_{QS}(0)W(s) + \int_0^s \frac{d\Gamma_{QS}(\sigma)}{d\sigma} W(s-\sigma) d\sigma) \qquad (10)$$

where Γ_{QS} is the quasi-steady circulation. It should be noted that the above-mentioned equation reduces to all previous forms of Duhamel's integral for each specific case. This equation allows us to account for all the instantaneous effects, and this can be done by writing $\Gamma = \Gamma_{rot} + \Gamma_{trans}$. Using results from Fung [22] for a pitching airfoil, Γ_{rot} can be written as:

$$- \quad \Gamma_{rot} = \pi c^2 \dot{\alpha} \left(\frac{3}{4} - \hat{x}_o \right) \qquad (11)$$

The main assumption here is that the nonlinearity of the $C_L - \alpha$ curve is accounted for in in the input of the equation, which is the circulation, and this does now affect the temporal build-up of the circulatory lift as shown in figures (22), (23). In order to apply this model to stability purposes and control, the author wrote equation (10) in state space form. The author started by writing the finite space model approximation of the Wagner function for a constant U:

$$- \quad W(s) = 1 - A_1 e^{-b_1 s} - A_2 e^{-b_2 s} \qquad (12)$$

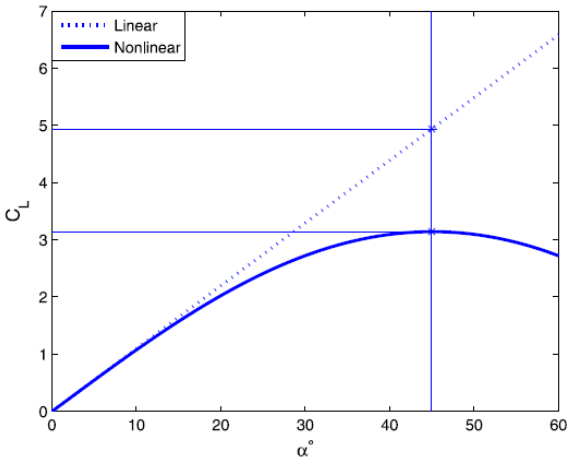

Fig. 22, taken from reference [23] linear/ nonlinear lift build up Vs. α

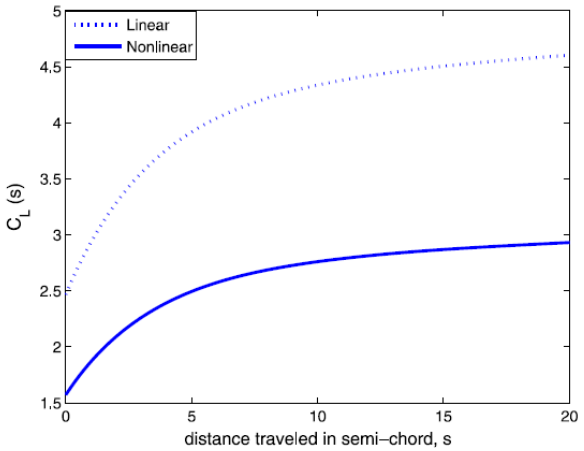

Fig. 23, taken from reference [23] linear/ nonlinear lift build up Vs. semi-chord s

The author then used Laplace transform to get a transfer function and then get the equivalent state space model. Writing Eq. (10) in terms of t and τ:

$$- \quad l(t) = \rho U(t) \Gamma_{eff}(t) = \rho U(t) (\Gamma_{QS}(t) W(0) - \int_0^t \frac{\Gamma_{QS}(\tau) dW(t-\tau)}{d\tau} d\tau \qquad (13)$$

where Γ_{eff} is the effective unsteady circulation. Using the finite state approximation of the Wagner function presented in Eq. (12):

$$- \quad \frac{dW(t-\tau)}{d\tau} = -\frac{A_i 2b_i}{c} U(\tau) e^{-\frac{2b_i}{c}\int_\tau^t U(\tau)d\tau}, \ \ i = 1,2 \qquad (14)$$

$$- \quad \Gamma_{eff}(t) = (1 - A_1 - A_2)\Gamma_{QS}(t) + x_i(t), \ \ i = 1,2 \qquad (15)$$

where $x_i(t)$ is:

$$- \quad x_i(t) = \int_0^t \frac{\Gamma_{Qs}(\tau) A_i 2b_i}{c} U(\tau) e^{-\frac{2b_i}{c}\int_\tau^t U(\tau)d\tau} d\tau, \ \ i = 1,2 \qquad (17)$$

This equation represents the solution for:

$$- \quad \dot{x_i}(t) = \frac{2b_i U(t)}{c}\Big(-x_i(t) + A_i \Gamma_{Qs}(t)\Big), \ \ i = 1,2 \qquad (18)$$

This is basically an ordinary differential equation with an initial condition of $x_i(0) = 0$. Finally, the lift can be written as:

$$- \quad l(t) = \rho U(t)[(1 - A_1 - A_2)\Gamma_{Qs} + x_1(t) + x_2(t)] \qquad (19)$$

where the state equation is Eq. (), and Γ_{qs} is written as:

$$- \quad \Gamma_{QS} = \frac{1}{2} c U(t) C_{L,s}\big(\alpha(t)\big) + \pi c^2 (\frac{3}{4} - \widehat{x_0}) \qquad (20)$$

The developed model requires the static lift curve to be known. As mentioned in the previous sections, the quasi-steady C_L equation developed by Dickinson has been used extensively (refer to sections 2.1 and 2.2). However, this model does not account for any wing geometry variation. The author used the *Extended lifting line theory* to obtain:

$$- \quad C_{L\alpha} = \frac{\pi AR}{1+\sqrt{\left(\frac{\pi AR}{a_0}\right)^2+1}} \qquad (21)$$

where $AR = \frac{R^2}{S}$ and a_0 is the lift curve slope of a two-dimensional airfoil section. Using conventional lift curves, we can write a_O as:

$$- \quad C_L = \frac{\pi AR}{2(1+\sqrt{\left(\frac{\pi AR}{a_0}\right)^2+1})} sin2\alpha \qquad (22)$$

Lastly, the total lift can be written as the sum of circulatory lift and non-circulatory lift as:

$$- \quad l(r,t) = l_{NC}(r,t) + \rho r|\dot{\varphi}(t)|[(1-A_1-A_2)\Gamma_{Qs}(r,t) + x_1(r,t) + x_2(r,t)] \qquad (23)$$

where U is written as $r\dot{\varphi}(t)$ given that $\varphi(t)$ is the flapping angle about the z_b axis.

The kinematics of the flapping bird is explained explicitly in the paper. As mentioned in the introduction, the author validated his model with CFD done by Sun and Du in [24]. Here are the results:

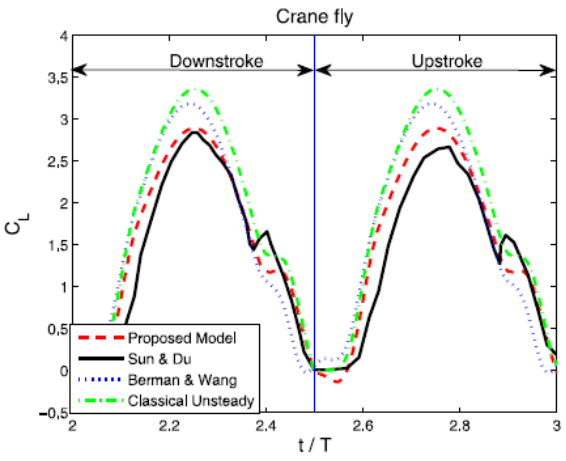

Fig. 24, taken from reference [23] Cranefly lift curve at f = 45.5 Hz and α_m= 30

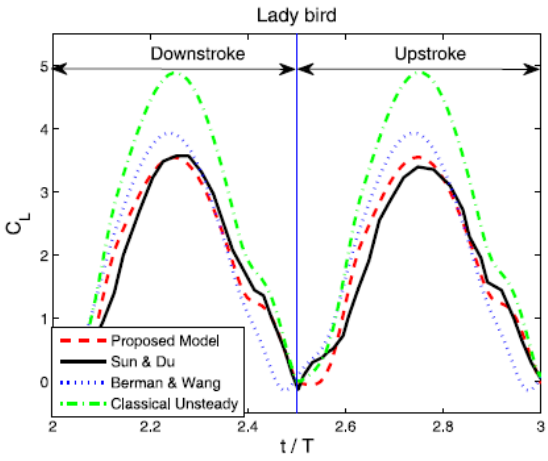

Fig. 25, taken from reference [23] Ladybird lift curve at f = 54 Hz and α_m= 43

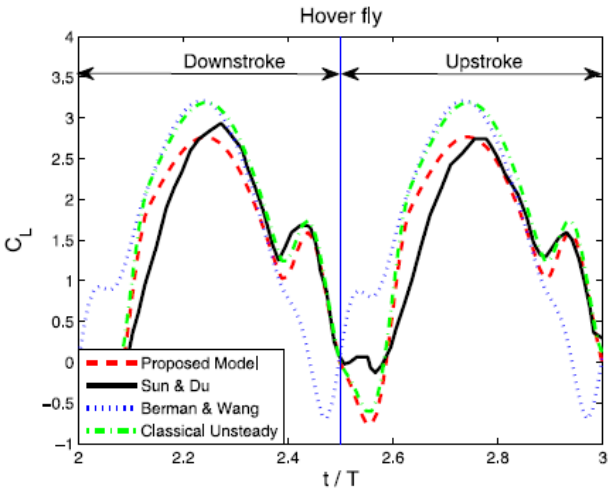

Fig. 26, taken from reference [23] Hoverfly lift curve at f = 160 Hz and α_m= 29

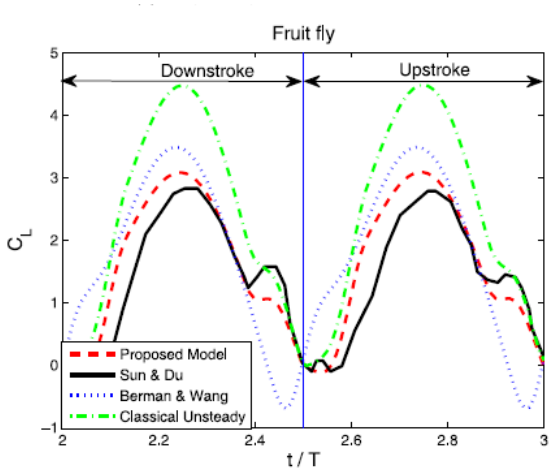

Fig. 27, taken from reference [23] Fruit fly lift curve at f =254 Hz and α_m= 46

In conclusion, as seen from the results in figures (24, 25, 26,27), the unsteady model proposed by Taha in [23] greatly matches the CFD results, and predicts the unconventional flight mechanisms that increase the force of a flapping flyer, such as the LEV.

Chapter 3

Longitudinal Flight dynamics

In this chapter, we will be discussing two papers written by Taha, [34] and [21]. The first chapter will be concerned with the longitudinal flight dynamics and how it is incorporated with quasi-steady modeling. The derived flight dynamics will then be assessed for its stability using averaging techniques. The second chapter will be concerned with the groundbreaking work of Taha on the insect's vibrational stabilization during hover, a problem that has been in question for more than two decades.

3.1 Longitudinal Flight dynamics of Hovering MAVs/insects

In this paper, the focus in on longitudinal motion, so only pitching rotation θ is considered. There are two frames that will be used to get the model, a body-fixed frame and a wing-fixed frame. The insect model considered are those of the horizontal stroke plane family.

The author assumed that there is no out of plane motion. Here is a schematic of for a flapping MAV:

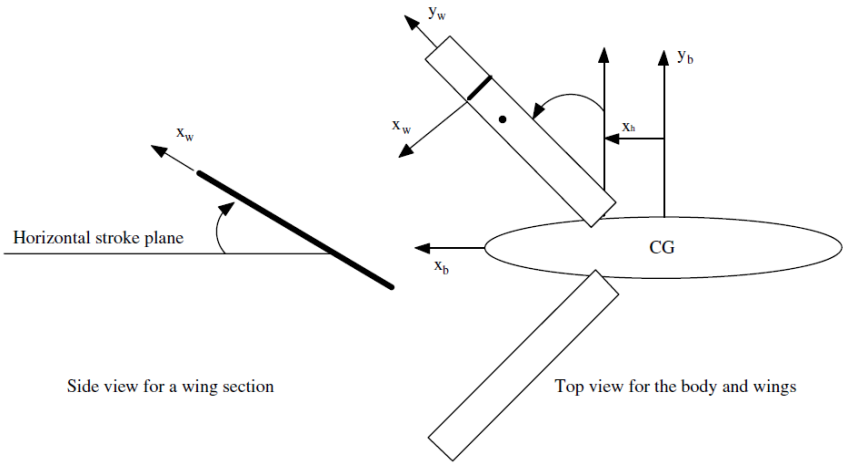

Fig. 28, taken from reference [34] Schematic diagram of a hovering MAV in a horizontal stroke plane.

The derivation starts with laying out the longitudinal dynamics of a conventional aircraft:

$$\begin{bmatrix} \dot{u} \\ \dot{w} \\ \dot{q} \\ \dot{\theta} \end{bmatrix} = \begin{bmatrix} -qw - gsin\theta \\ qu + gcos\theta \\ 0 \\ q \end{bmatrix} + \begin{bmatrix} \frac{1}{m}X \\ \frac{1}{m}Z \\ \frac{1}{I_y}M \\ 0 \end{bmatrix} \tag{24}$$

or in vector form as $\dot{\boldsymbol{x}} = \boldsymbol{f}(\boldsymbol{x}) + \boldsymbol{g_a}(\boldsymbol{x}, \boldsymbol{t})$, where g is the gravitational acceleration, m is the body mass, and I_y is the body moment of inertia around the y_b axis. $\boldsymbol{x}$ is out state variable, with $\boldsymbol{x} = [u, w, q, \theta]^T$. u is the center of mass velocity in the x_b direction, w is the center of mass velocity in the z_b direction, θ is the pitching angle about the y_b axis, and q is the angular velocity about the y_b axis.

In the previous chapter, we explored the papers by Taha and Dickinson in their analysis and modeling of flapping wings. We will not be going into many details regarding

aerodynamic analysis in this chapter. Taha used a quasi-steady model in his aerodynamic analysis in this work. C_L was showed by Wang in [27] that in can be written as:

$$- \quad C_L = A\, sin2\alpha \qquad (25)$$

Taha showed in [23] (details are summarized in section 2.3) that A can be written as:

$$- \quad A = \frac{\pi AR}{2[1+\sqrt{\left(\frac{\pi AR}{a_0}\right)^2+1}]} \qquad (26)$$

And also, that C_D can be written as:

$$- \quad C_D = C_L tan\alpha = 2Asin^2\alpha \qquad (27)$$

It was shown by Dickinson in [28] (also in section 2.2) that the experiments are very close to the theoretical results for the Γ_{rot} if written as:

$$- \quad \Gamma_{rot} = \pi c^2 \dot{\eta}(\tfrac{3}{4} - \hat{x}_0) \qquad (28)$$

where c is the chord length, $\dot{\eta}$ is the pitching angular velocity of the wing, and $\hat{x}_0$ is the normalized chord position of the pitch axis from the leading edge. Using the preceding equations, for an airfoil section a distance r from the wing root:

$$- \quad l(r,t) = \tfrac{1}{2}\rho Ac(r)U^2(r,t)sin2\alpha(r,t) + \pi\rho\left(\tfrac{3}{4} - \hat{x}_0\right)U(r,t)c^2(r)\eta(\dot{t}) \qquad (29)$$

$$- \quad d(r,t) = \rho Ac(r)U^2(r,t)\sin^2\alpha\,(r,t) \qquad (30)$$

where U is the velocity of the wing section relative to the air.

Next, the author went on to incorporate the dynamic model into the aerodynamic model. For that to be done, the effects of the body motion variables on U should be included:

- $U = \sqrt{(r\dot{\varphi} + ucos\varphi)^2 + w^2}, where\ \alpha = \alpha_\eta + \alpha_i\ and\ \dot{\eta} \longrightarrow \dot{\eta} + qcos\varphi$ (31)

where α_η and α_i can be written as:

- $\alpha_\eta(t) = \begin{cases} \eta, & U > 0 \\ \pi - \eta, & U < 0 \end{cases}$ and $\alpha_i = \tan^{-1}\frac{w - q(rsin\varphi + x_h)}{U}$ (32)

where α_η and α_i are the angles of attacked induced by the wing pitch angle and the angle of attack induced by the body motion, respectively. We can now write the lift and drag per unit span as:

- $l(\boldsymbol{x}, t; r) = \frac{1}{2}\rho Ac(r)U^2\left[sin2\alpha_\eta(t) + 2cos\alpha_\eta(t)\frac{w_{eff}(\boldsymbol{x},t;r)}{|U(\boldsymbol{x},t;r)|}\right] + \pi\rho\left(\frac{3}{4} - \hat{x}_0\right)c^2(r)U(\boldsymbol{x}, t; r)[\dot{\eta}(t) + qcos\varphi(t)]$ (33)

- $d(\boldsymbol{x}, t; r) = \rho Ac(r)U^2(\boldsymbol{x}, t; r)[\sin^2\alpha_\eta(t) + sin2\alpha_\eta(t)\frac{w_{eff}(\boldsymbol{x},t;r)}{|U(\boldsymbol{x},t;r)|}$ (34)

where $w_{eff} = w - q(rsin\varphi + x_h)$. We can now write the flight dynamics model as:

$$\begin{bmatrix}\dot{u}\\ \dot{w}\\ \dot{q}\\ \dot{\theta}\end{bmatrix} = \begin{bmatrix}-qw - gsin\theta\\ qu + gcos\theta\\ 0\\ q\end{bmatrix} + \begin{bmatrix}\frac{1}{m}X_0\\ \frac{1}{m}Z_0\\ \frac{1}{I_y}M_0\\ 0\end{bmatrix} + \begin{bmatrix}X_u & X_w & X_q & 0\\ Z_u & Z_w & Z_q & 0\\ M_u & M_w & M_q & 0\\ 0 & 0 & 0 & 0\end{bmatrix}\begin{bmatrix}u\\ w\\ q\\ \theta\end{bmatrix} \quad (35)$$

where for $\dot{\eta} = 0$, i.e., no change in the wing pitch angle, we have:

- $X_0(t) = -2K_{21}\dot{\varphi}(t)|\dot{\varphi}(t)|cos\,\varphi(t)sin2\,\eta\,, \quad Z_0(t) = -K_{21}\dot{\varphi}(t)|\dot{\varphi}(t)|\,sin\,2\eta$ (36)

- $M_0(t) = 2\dot{\varphi}(t)|\dot{\varphi}(t)| \sin\eta[K_{22}\widehat{\Delta x}\cos\phi(t) + K_{21}x_h\cos\eta(t) + K_{32}\sin\varphi(t)\cos\eta]$ (37)

where $K_{mn} = \frac{1}{2}\rho A I_{mn}$ and $I_{mn} = 2\int_0^R r^m c^n(r)dr$. As for the time-varying stability derivatives:

$$X_u = -\frac{4K_{11}}{m}|\dot{\varphi}|\cos^2\varphi\sin^2\eta, \qquad X_w = -\frac{K_{11}}{m}|\dot{\varphi}|cos\varphi sin2\eta$$

$$X_q = \frac{K_{21}}{m}|\dot{\varphi}|sin\varphi\ cos\varphi\ sin2\eta - x_h X_w, \qquad Z_u = 2X_w$$

$$Z_w = -\frac{2K_{11}}{m}|\dot{\varphi}|\cos^2\eta, \qquad Z_q = \frac{2K_{12}}{m}|\dot{\varphi}|sin\varphi\cos^2\eta - \frac{K_{rot_{12}}}{m}\dot{\varphi}cos\varphi - x_h Z_w \quad (36)$$

$$M_u = \frac{4K_{12}\Delta x}{I_y}|\dot{\varphi}|\cos^2\varphi\ \ sin\eta + \frac{m}{I_y}\left(2X_q - x_h Z_u\right), \qquad M_w = \frac{2K_{12}\Delta x}{I_y}|\dot{\varphi}|cos\varphi\ cos\eta + \frac{2K_{21}}{I_y}|\dot{\varphi}|sin\varphi\cos^2\eta - \frac{mx_h}{I_y}Z_w$$

$$M_q = -\frac{2\Delta x}{I_y}|\dot{\varphi}|cos\varphi\ cos\eta\ (K_{12}x_h + K_{22}sin\varphi) + \frac{1}{I_y}\dot{\varphi}cos\varphi(K_{rot_{13}}\Delta x\ cos\varphi\ cos\eta + \left(K_{rot_{22}}\ sin\varphi\right) - \frac{2}{I_y}|\dot{\varphi}|\cos^2\eta\ \ sin\varphi(K_{21}x_h + K_{31}sin\varphi) - \frac{K_v\mu_1 f}{I_y}\cos^2\varphi - \frac{mx_h}{I_y}Z_q$$

Where $K_{rot} = \pi\rho\left(\frac{1}{2} - \Delta\hat{x}\right)I_{mn}$, $K_v = \frac{\pi}{16}\rho I_{04}$.

The preceding model has been tested for stability and validated with results from benchmark results from Sun at [28].

In the stability analysis, the authors applied the averaging theorem. The averaging theorem can be written in the form of:

- $\dot{\bar{\boldsymbol{X}}} = \epsilon\bar{\boldsymbol{f}}(\bar{\boldsymbol{X}})$

Where $\bar{\boldsymbol{f}}(\boldsymbol{X}) = \frac{1}{T}\int_0^1 (\boldsymbol{X}, \tau)\, d\tau$. According to the averaging theorem, if ϵ is small enough, then the exponential stability of the averaged system concludes the potential stability of the NLTP system.

Applying the averaging theorem to our original system, it can be written in the following form:

$$\dot{\bar{\boldsymbol{X}}} = \begin{pmatrix} \dot{\bar{u}}(t) \\ \dot{\bar{w}}(t) \\ \dot{\bar{q}}(t) \\ \dot{\bar{\theta}}(t) \end{pmatrix} = \begin{pmatrix} -\bar{q}(t)\bar{w}(t) - g\sin(\bar{\theta}(t)) \\ \bar{q}(t)\bar{u}(t) + g\cos(\bar{\theta}(t)) \\ 0 \\ \bar{q}(t) \end{pmatrix} + \begin{pmatrix} \frac{1}{m}\overline{X_0} \\ \frac{1}{m}\overline{Z_0} \\ \frac{1}{I_y}\overline{M_0} \\ 0 \end{pmatrix} + \begin{bmatrix} \overline{X_u} & \overline{X_w} & \overline{X_q} & 0 \\ \overline{Z_u} & \overline{Z_w} & \overline{Z_q} & 0 \\ \overline{M_u} & \overline{M_w} & \overline{M_q} & 0 \\ 0 & 0 & 0 & 0 \end{bmatrix} \begin{pmatrix} \bar{u}(t) \\ \bar{w}(t) \\ \bar{q}(t) \\ \bar{\theta}(t) \end{pmatrix} \tag{37}$$

The nice thing about the averaging theorem is that it converts the nonlinear time periodic system, into an autonomous equation such as the one in equation (37). Now, the process of finding a periodic orbit is reduced to finding a fixed point of the averaged system. The trim conditions for hovering of insects now are:

$$\overline{X_0} = 0, \quad -\overline{Z_0} = \overline{L_0} = mg, \quad \overline{M_0} = 0 \tag{38}$$

The stability of the trimmed system was tested, and the results were validated with those by Sun [29]. Here are the results:

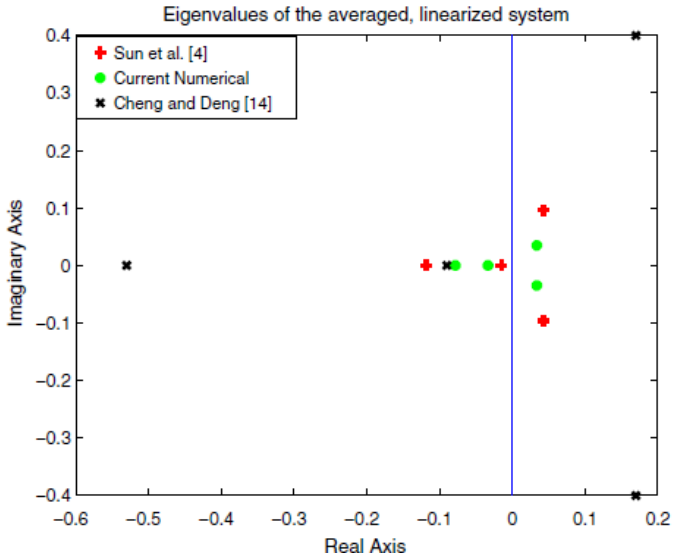

Fig. 29, taken from reference [34] Eigenvalues of the averaged linear dynamics compared with Sun, and Cheng and Deng's model

As can be seen, the model results are very close to the results by Sun than those of Cheng. The deviation of the results of Cheng may be caused by Cheng's model ignoring of rotational effects. Finally, these results are very well known in the flapping flight community. The LTI system eigenvalue structure has two stable non-oscillatory modes and an unstable oscillatory mode. So, the system is rendered as unstable. Is this really the case? Or is it only because averaging does not show the whole range of dynamics? It appeared that actually insects have vibrational stabilization, that there is no feedback action needed. Also, the first order averaging was not enough in showing the whole dynamic spectrum of insects. This is what Taha discovered in his groundbreaking work in [21]. That insects have its own stability characteristics inherited in a vibrational stabilization mechanism.

3.2 Vibrational stabilization

Applying direct averaging on equation (24) and linearizing about the hovering equilibrium, it can be written as:

$$\dot{\begin{pmatrix} \bar{u} \\ \bar{w} \\ \bar{q} \\ \bar{\theta} \end{pmatrix}} = \begin{bmatrix} \overline{X_u} & 0 & 0 & -g \\ 0 & \overline{Z_w} & 0 & 0 \\ \overline{M_u} & 0 & \overline{M_q} & 0 \\ 0 & 0 & 1 & 0 \end{bmatrix} \begin{pmatrix} \bar{u} \\ \bar{w} \\ \bar{q} \\ \bar{\theta} \end{pmatrix} \qquad (39)$$

where the bar over the variables indicates average quantity of the aerodynamic stability derivative. The function of each stability derivative is embedded in its name. For instance, Z_w is the change in Z force due to a disturbance w. As mentioned in the last section, this system has two stable oscillatory modes and an unstable oscillatory mode that comes from

the complex conjugate pair of eigenvalues with a positive real part, which concludes the instability of the system. This instability comes from the absence of an M_θ term. That is, there is no moment that restores the insect to its original position due to a disturbance in θ. However, Taha revealed that in using higher order averaging and chronological calculus, such term exists [21].

Agrachev and Gamkrelidze were the ones who developed a new calculus for time varying dynamical systems: the chronological calculus [30]. Sarychev in [31] introduced the concept of higher order averaging:

$$\dot{\boldsymbol{X}} = \epsilon\bar{\boldsymbol{f}}(\bar{\boldsymbol{X}}) = \epsilon\boldsymbol{\Lambda}_1(\bar{\boldsymbol{X}}) + \epsilon^2\boldsymbol{\Lambda}_2(\bar{\boldsymbol{X}}) + \epsilon^3\boldsymbol{\Lambda}_3(\bar{\boldsymbol{X}}) + \cdots \qquad (40)$$

where:

$$\boldsymbol{\Lambda}_1(\boldsymbol{X}) = \frac{1}{T}\int_o^T \boldsymbol{F}(\boldsymbol{X}, t)dt \quad (41)$$

$$\boldsymbol{\Lambda}_2(\boldsymbol{X}) = \frac{1}{2T}\int_o^T \left[\int_o^T \boldsymbol{F}(\boldsymbol{X}, \sigma)d\sigma, \boldsymbol{F}(\boldsymbol{X}, t)\right] dt \quad (42)$$

$$\boldsymbol{\Lambda}_3(\boldsymbol{X}) = -\frac{T}{2}[\boldsymbol{\Lambda}_1(\boldsymbol{X}), \boldsymbol{\Lambda}_2(\boldsymbol{X})] + \frac{1}{3T}\int_o^T [\int_o^T \boldsymbol{F}(\boldsymbol{X}, \sigma)d\sigma, \left[\int_o^T \boldsymbol{F}(\boldsymbol{X}, \sigma)d\sigma, \boldsymbol{F}(\boldsymbol{X}, t)\right]]dt \quad (43)$$

where [,] is the lie bracket operation which is:

$$[\boldsymbol{U_1}, \boldsymbol{U_2}] = \frac{\partial \boldsymbol{U_2}}{\partial \boldsymbol{X}}\boldsymbol{U_1} - \frac{\partial \boldsymbol{U_1}}{\partial \boldsymbol{X}}\boldsymbol{U_2} \qquad \mathbf{(44)}$$

In the complete averaged dynamics in Eq (41), $\boldsymbol{\Lambda}_1(\boldsymbol{X})$ is the first order averaging terms. As can be seen from Eq (40), if ϵ us small enough, the second and third average dynamics will vanish. Applying these concepts on the hawkmoth system, we have:

- $\frac{\partial \mathbf{\Lambda_1}}{\partial \boldsymbol{x}}(0) = \begin{bmatrix} -3.59 & 0 & 0 & -9.81 \\ 0 & -3.3 & 0 & 0 \\ 39.95 & 0 & -7.92 & 0 \\ 0 & 0 & 1 & 0 \end{bmatrix}$, (45)

Emergence of the M_θ term

- $\frac{\partial (\mathbf{\Lambda_1}+\mathbf{\Lambda_2})}{\partial \boldsymbol{x}}(0) = \begin{bmatrix} -3.58 & 0 & 0 & -9.81 \\ 0 & -3.09 & 0 & 0 \\ 29.98 & 0 & -8.13 & -28.45 \\ -2.9 & 0 & 0.96 & 0 \end{bmatrix}$ (46)

This higher order averaging resulted in the shifting of the eigen values to being a completely stable system. Taha, using chronological calculus, derived the following equation for vibrationally induced pitch stiffness for insect flight dynamics:

- $k_\theta = \frac{g}{2T} \int_o^T \left[M_{V_x}(t)dt - \int_o^\tau M_{V_x}(\tau)d\tau \right] dt$ (47)

where T is the flapping period, and M_{V_x} is the change of pitching moment due to the velocity $V_x = u\cos\theta + w\sin\theta$. Equation (47) simply tells us that k_θ is related to two phenomena: gravity and cycle variation. For a constant M_{V_x}, like a non-oscillatory system such as fixed wing, k_θ would vanish. As all stability derivatives, k_θ can be decomposed to $\overline{M_{V_x}}$ and ΔM_{V_x}. The oscillation of the latter comes from the change in positions between the body center of gravity and the center of pressure of the wing. The following figure shows

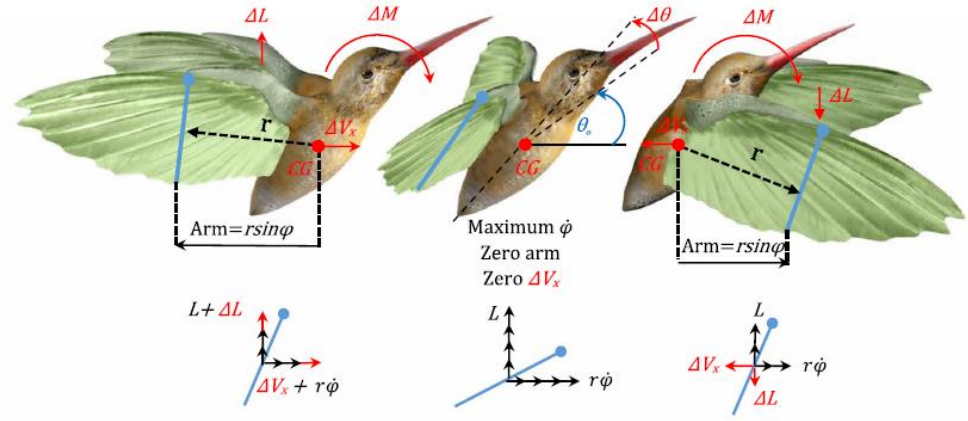

Fig. 30, taken from reference [34] illustration of the vibrational stabilization mechanism, and how the moment arm plays a role.

how the stabilization occurs due to the fact that the moment arm oscillates with respect to the CG.

Chapter 4

Experimental study

4.1 Motivation

The ADCL at UCI under supervision of Professor Haithem Taha is in the development of a new flying concept: a quad-flapping drone. The lab is aiming to utilize all the mentioned concepts in order to exploit this novel configuration. Up until now, the ADCL lab had a proof of concept for this flying machine. Our current objective is to develop an optimal design such as to make use of unsteady phenomena such as the clap and fling and delayed stall in how they can augment thrust. In order to do this, we need to know at which phase of the stroke to each phenomenon uniquely happens.

4.2 Experimental setup

The first part of the experimental apparatus is the 4-winged FWMAV, with a chassis of a crank-rocker mechanism that enables it to transmit rotational motion coming from the motor and gears. The mechanism is shown in figure ():

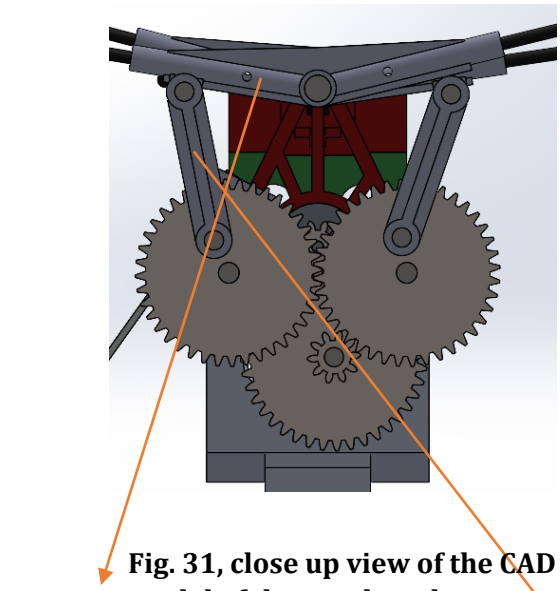

Fig. 31, close up view of the CAD model of the crank rocker mechanism.

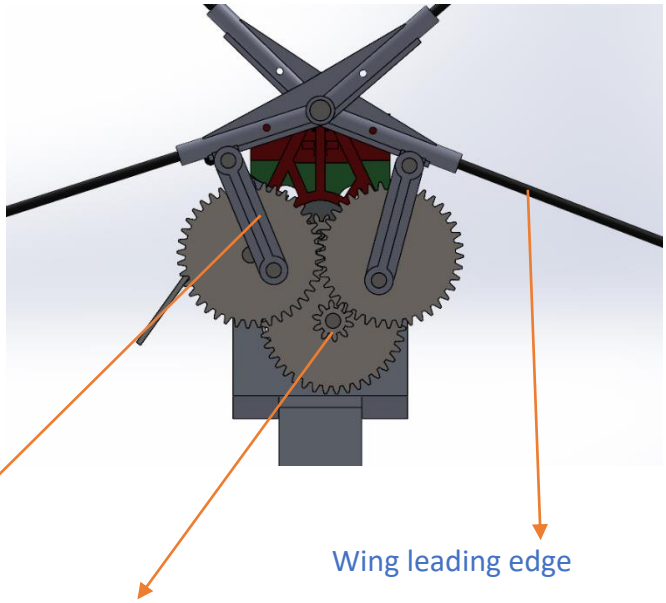

Fig. 32, close up view of the CAD model of the crank rocker mechanism at max φ

The mechanism is fabricated so that the output angle follows a near-sine waveform with time. The position loop equation of the rocker was derived by my senior colleague Moatasem Fouda, and a comparison with the sine wave form was made:

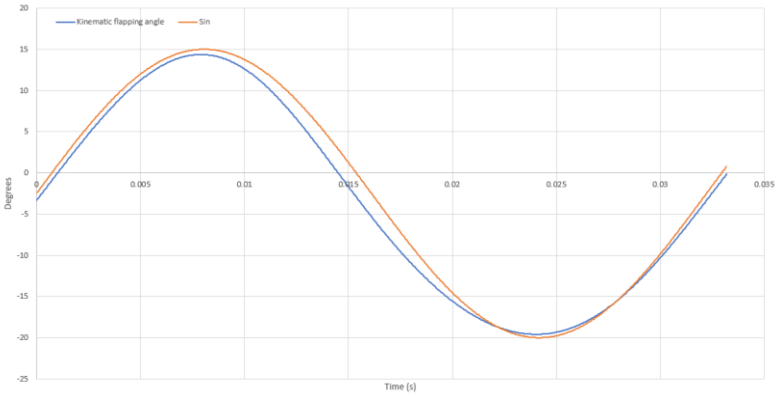

Fig. 33, the derivation of the kinematic flapping angle, and the closeness it is to a sin wave form

This resemblance will help us see how the forces vary with time as we can just input the sinusoidal wave for ease of calculation and use. The function used will be of the form: $\sin(\omega t - \varphi)$, where $\omega = 2\pi f$ for flapping frequency f and φ as the phase difference, i.e., the angle in which the bird was on at the beginning of each experiment.

The whole system relies on only one DC brushless motor with peak power of around 2.5 - 3 W with load. And can go up to 4 W without load. The gears are an 0.3 module, with gear ratio of 10:40.

The wings are elliptic wings, made from paper. The dimensions of the wings are $b = 140\ mm, a = 95\ mm$, where a and b are the semi minor axis and semi major axis, respectively, as shown in the figure ():

Fig. 34, ellipting wing planform used.

There are 4 wings, each attached to the carbon fiber rod coming out of the rocker as mentioned. The area of each wing is calculated as $A = 0.25\pi ab$. The area of one wing is equal to $10446\ mm^2$. The a here corresponds to the maximum chord of the wing and b the semi span. The wings are completely flexible with no kind of support such as spar inside them. This fact is extremely important to the generation and augmentation of thrust. The flexibility fact will utilize the clapping mechanism and, as we will see, will be the main phenomenon behind the highest force production in a flapping cycle.

The second main part of the apparatus is the 4-axis load cell. The 4-axis load cell consists of 4 load cells attached together in a special way in which it can measure thrust, lift, moment around the x-axis, and moment around the y-axis. Before going any further, here is a picture that defines the axes of the load cell:

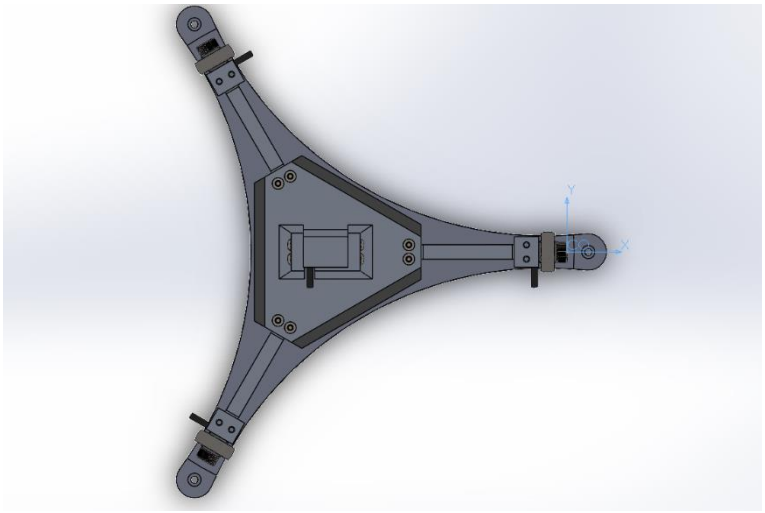

Fig. 35, top view of the 4 axis LC

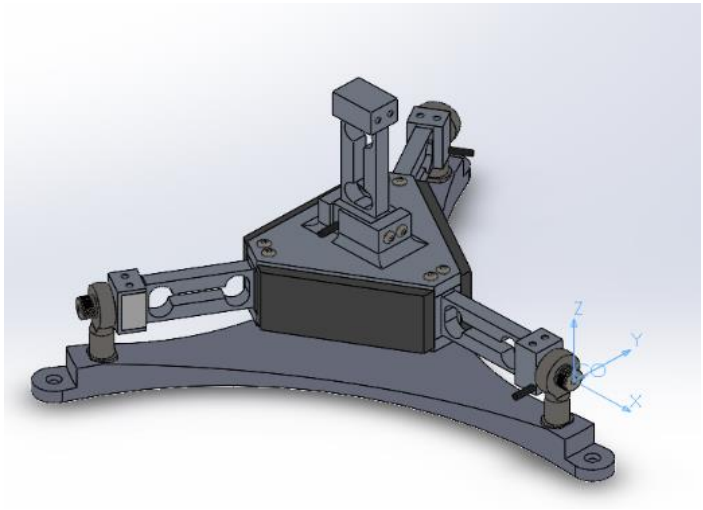

Fig. 36, full view of the 4-axis LC

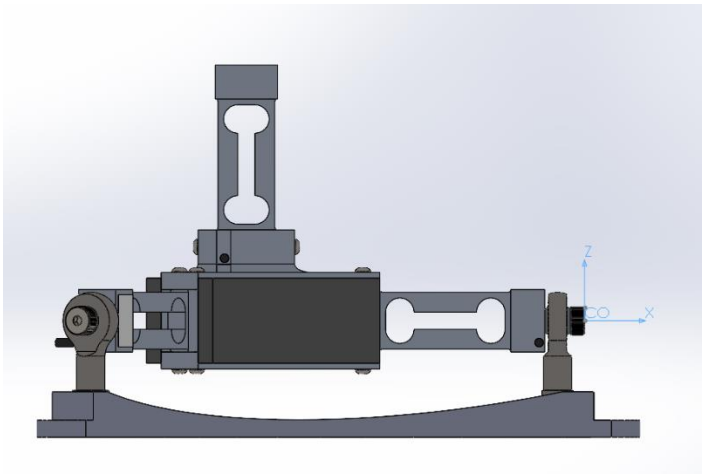

Fig. 37, side view of the 4 axis LC

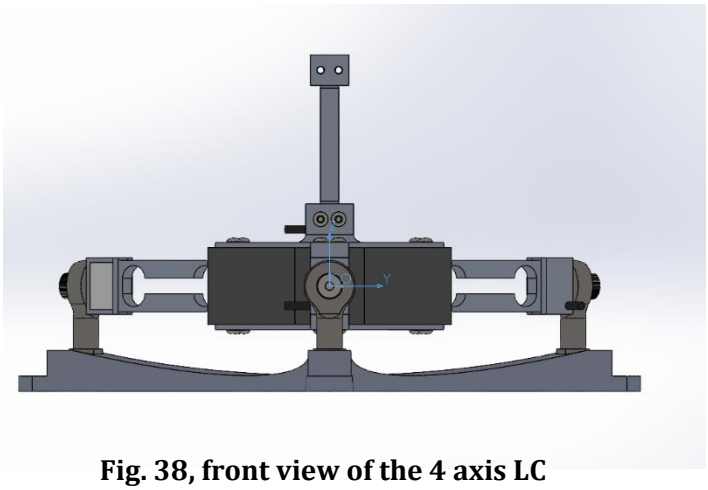

Fig. 38, front view of the 4 axis LC

This 4-axis load cell design was patented here in the lab, the design was made by my senior colleague Moatasem Fouda, more on this can be found here [42]. As mentioned, this design

is used to measure different forces and moments, captured using the LABVIEW software. The bird is attached on the vertical load cell, as demonstrated in the coming figure (40):

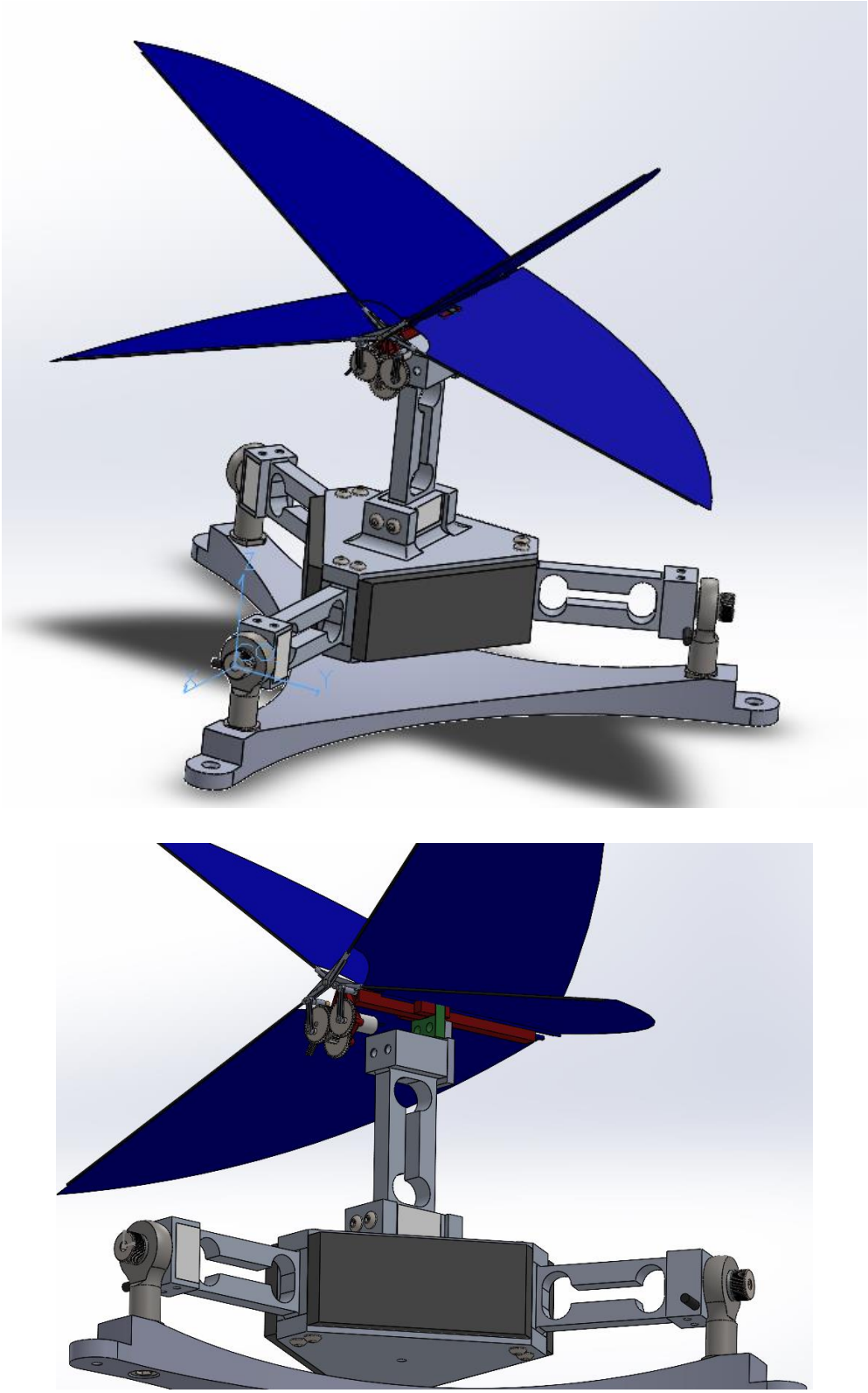

Fig. 39, full experimental setup

The forces measurements were acquired using NI 6211 DAQ assistant through LABVIEW program. The complete experimental apparatus is shown in figure ():

Fig. 40, block diagram for the measurements

In order to detect the frequency, a Hall sensor was attached on the chassis that gives a signal every time the wing reaches maximum flapping angle φ. The data is also acquired using the LABVIEW program and the frequency is calculated as the number of edges per $\frac{number\ of\ samples}{sampling\ rate}$. Forces and moments were measured for frequencies from 5 Hz up to 13 Hz with an increment of 0.5 Hz. All captured data with frequencies from 5-9.5 Hz were filtered using a digital low pass filter at a cutoff frequency of 2-3 times the flapping frequency. For frequencies of 10-13 Hz, an analogue low pass filter to make sure all the physics was captured. The analogue low pass filter was set at a cut off of 3 times or more of the flapping frequency and added to it a digital low pass filter at the same cut off frequency.

4.3 Results

4.3.1 Force and moment variation with flapping angle

As mentioned before, the Hall sensor was used to measure the frequency of the flapping wing. Not only that, its signal variation with time was also utilized to tell us when of the forces happen at what time. This will help us improve in the design of the new mechanism developed here at the ADCL lab.

The Hall sensor is attached at the side of the chassis, in which it gives a signal when the wing reaches maximum flapping angle φ at approximately 35 degrees. Zero degrees happen when the leading edges of the upper and lower wings clap with each other. The Hall sensor is wired to the power using a pull up resistor circuit, in which the default value it has is at 5 Volts. If the Hall sensor detects a magnet, the Hall sensor gives a 0 Volts measurement, in other words, it emits a signal in the LABVIEW software.

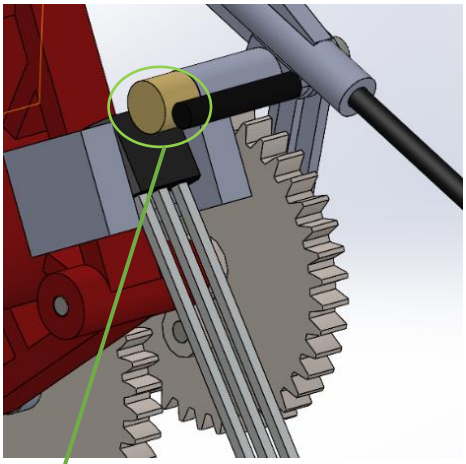

Fig. 41, close up view of the hall effect sensor and attached magnets.

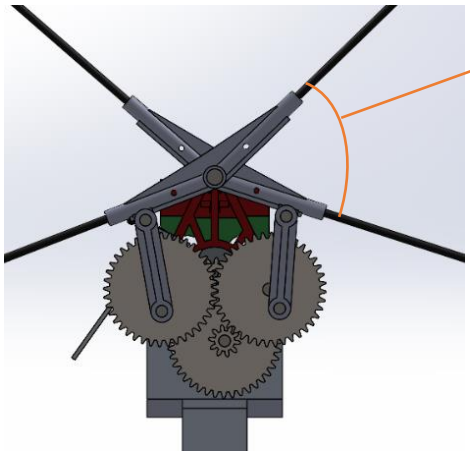

Fig. 42, mechanism at max φ

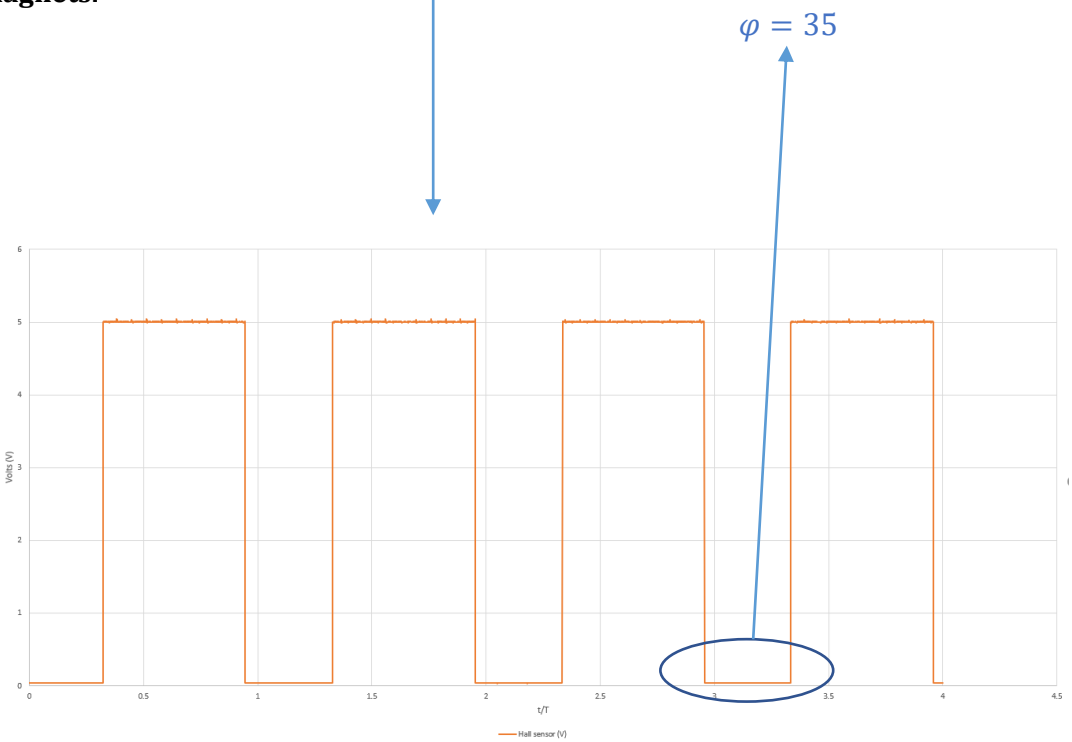

Fig. 43, Hall effect sensor signal into action, y-axis is volts, with t/T in x-axis.

As mentioned, since we now know from the kinematic property that the actual flapping angle is almost sin waveform, we have a position with time plot:

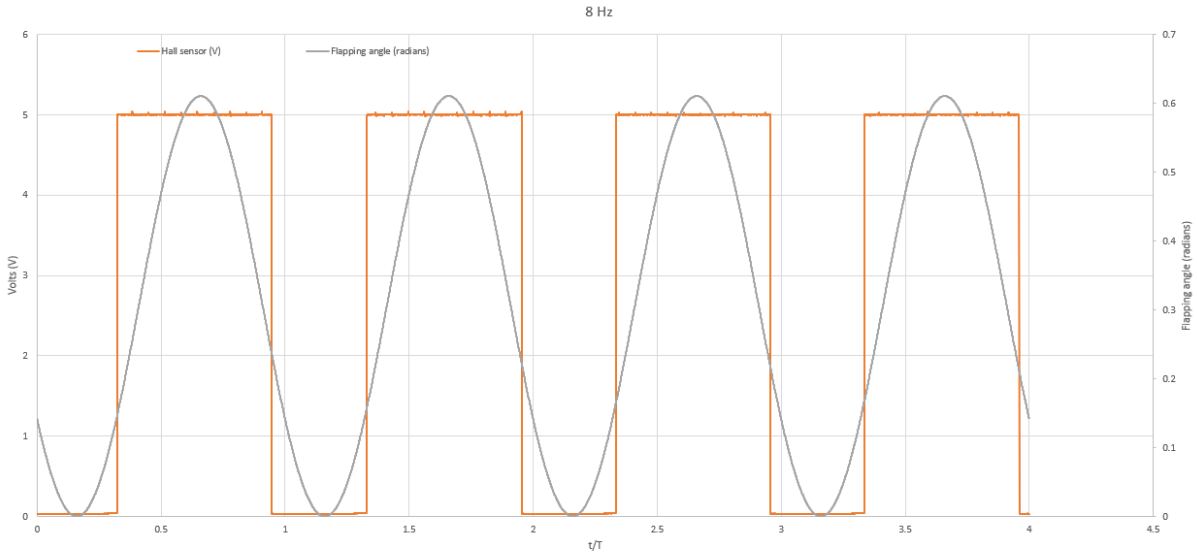

Fig. 44, alignment of the flapping angle with the hall sensor signal

One of the things to note here is the placement of the Hall sensor is imperfect, i.e., there is a small δt in which the Hall sensor detects the magnet before reaching the maximum flapping angle φ. The value of this δt is irrelevant since we know that in the way up, upstroke, whatever the δt is, the same δt will be detected in the downstroke also. This makes the approximation of the sin angle correct in the sense that the peak of the upstroke should be exactly at half length of the edge corresponding to it. So, any imperfection in placing the sensor on the chassis would not cause a big problem. Another thing to note is that compared, for instance, with the motion capture system for flapping angle capture, the hall effect sensor here is placed on the chassis, only the magnet with is less than 0.2 grams is on a rigid part of the wing. This results in that there will be no alteration in the dynamics/kinematics of the wing and thus of the whole system.

In the coming few pages, results of the thrust, lift, and pitching moment will be displayed with flapping angle for frequencies of 6-12 Hz. We will be discussing the results and the aerodynamics of thrust and lift and how in each position there us an underlying aerodynamic phenomenon that causes this behavior.

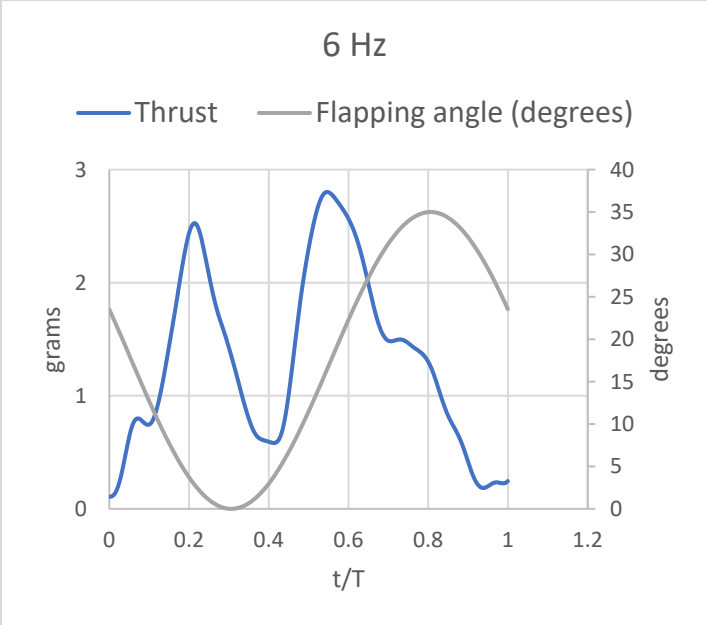

Fig. 45, thrust measurement with flapping angle Vs t/T at 6 Hz

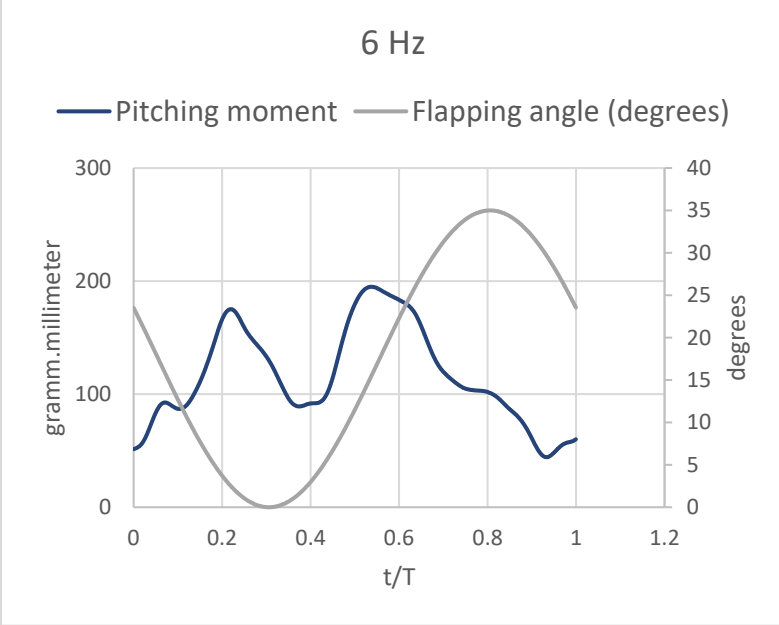

Fig. 46, Pitching moment measurement with flapping angle Vs t/T at 6 Hz

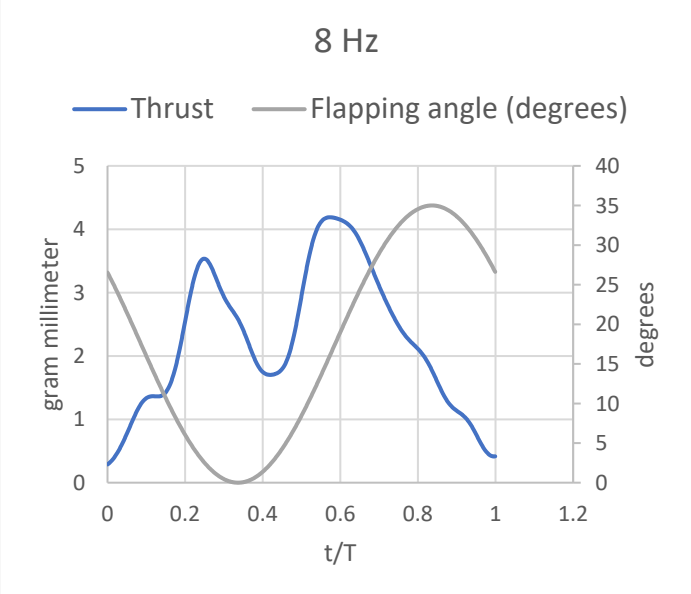

Fig. 47, thrust measurement with flapping angle Vs t/T at 8 Hz

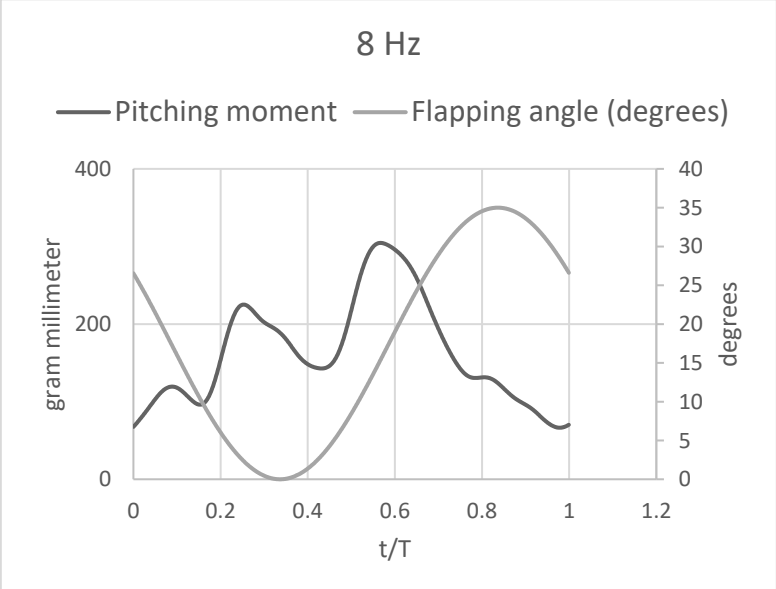

Fig. 48, Pitching moment measurement with flapping angle Vs t/T at 8 Hz

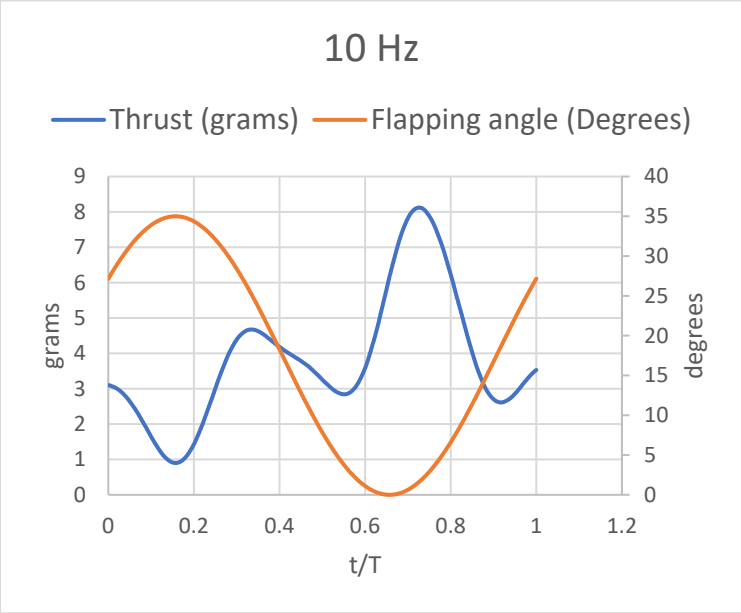

Fig. 49, thrust measurement with flapping angle Vs t/T at 10 Hz.

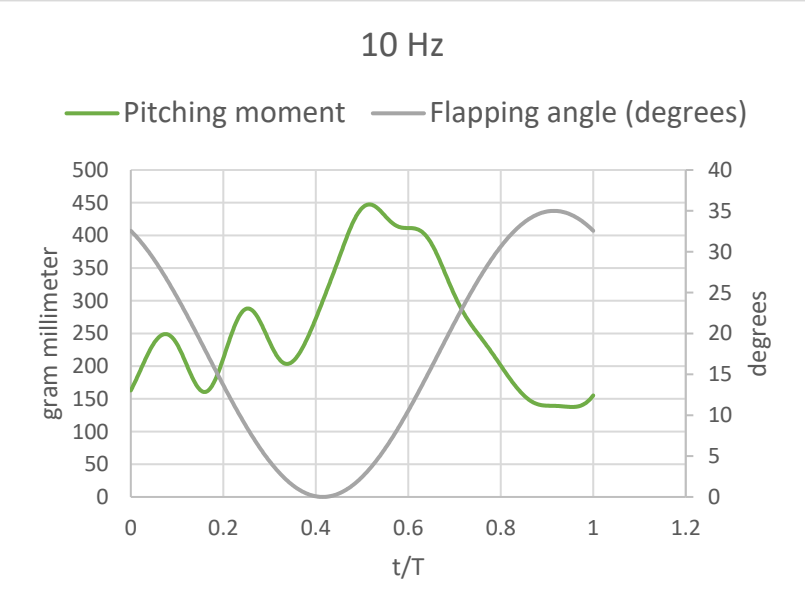

Fig. 50, Pitching moment measurement with flapping angle Vs t/T at 10 Hz

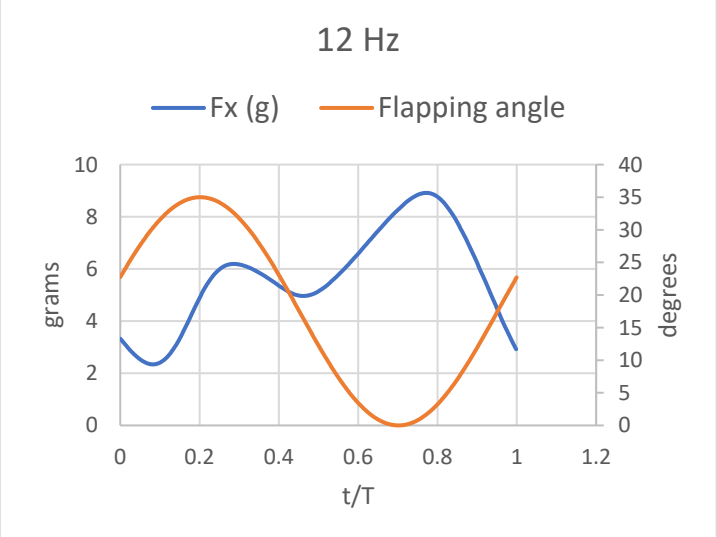

Fig. 51, thrust measurement with flapping angle Vs t/T at 12 Hz.

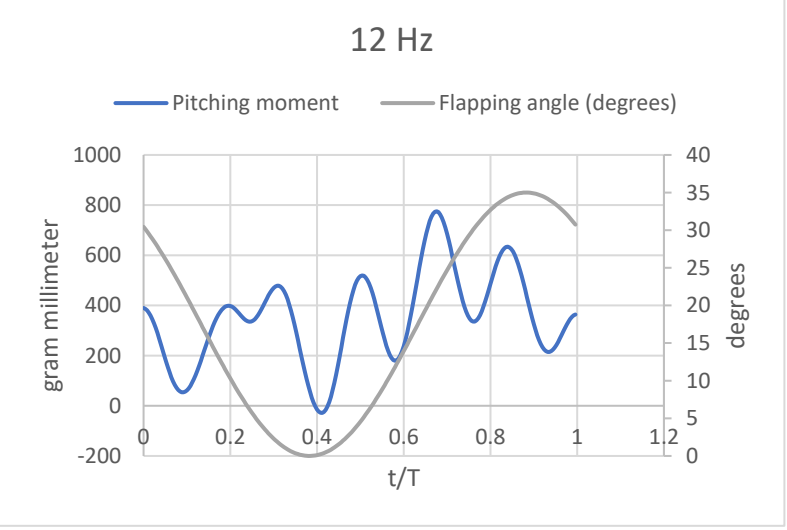

Fig. 52, Pitching moment measurement with flapping angle Vs t/T at 12 Hz.

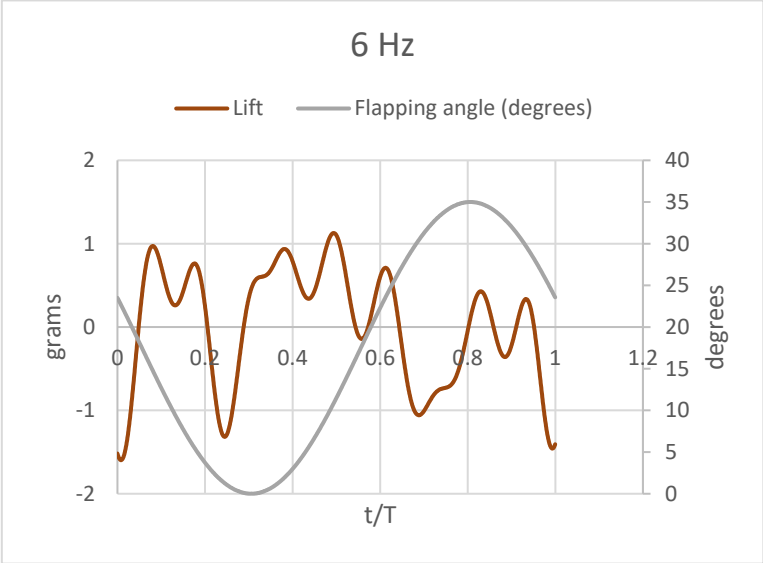

Fig. 53, Lift measurement with flapping angle Vs t/T at 6 Hz.

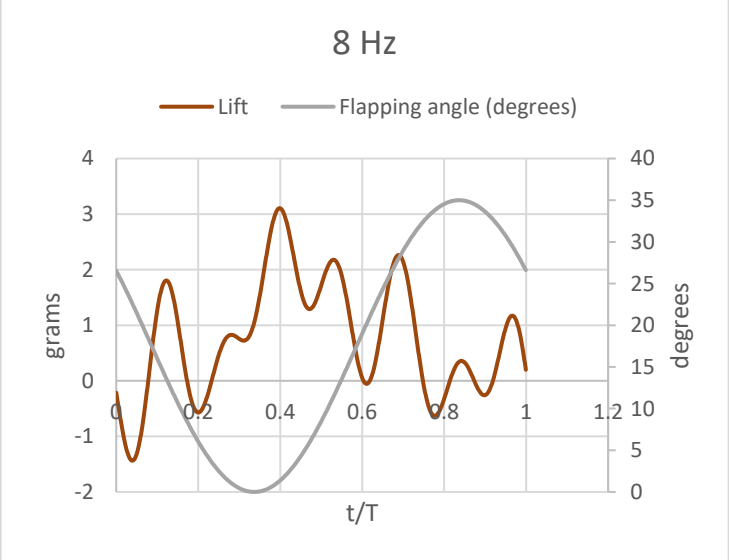

Fig. 54, Lift measurement with flapping angle Vs t/T at 8 Hz.

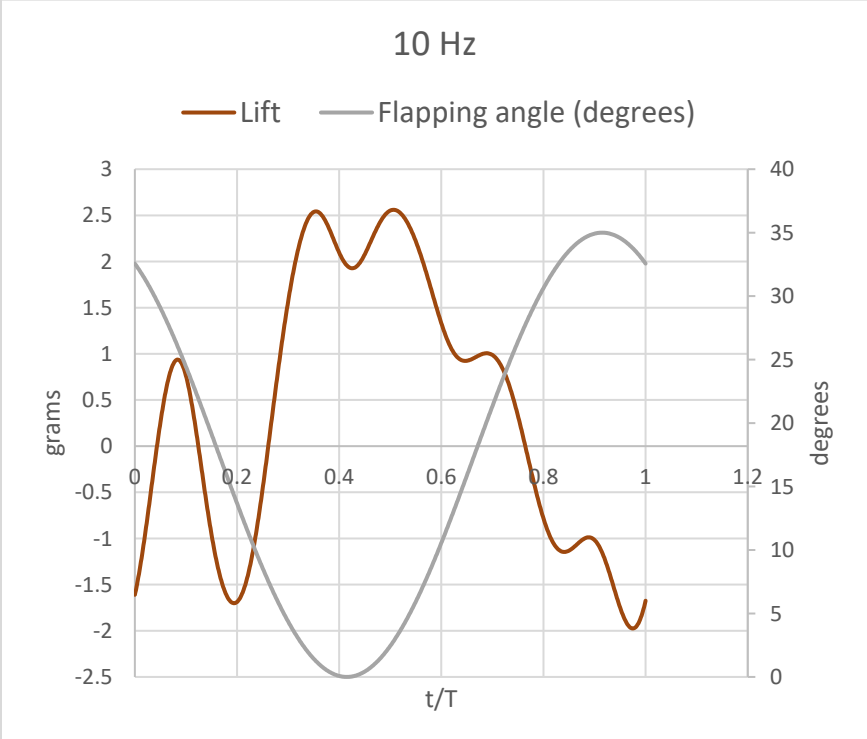

Fig. 55, Lift measurement with flapping angle Vs t/T at 10 Hz.

As has been highlighted before regarding the Hall sensor discussion, we will be calling the phase in which the wing goes from $\varphi = 35^o$ to zero the downstroke, and vice versa the upstroke. This is simulated in the following figure:

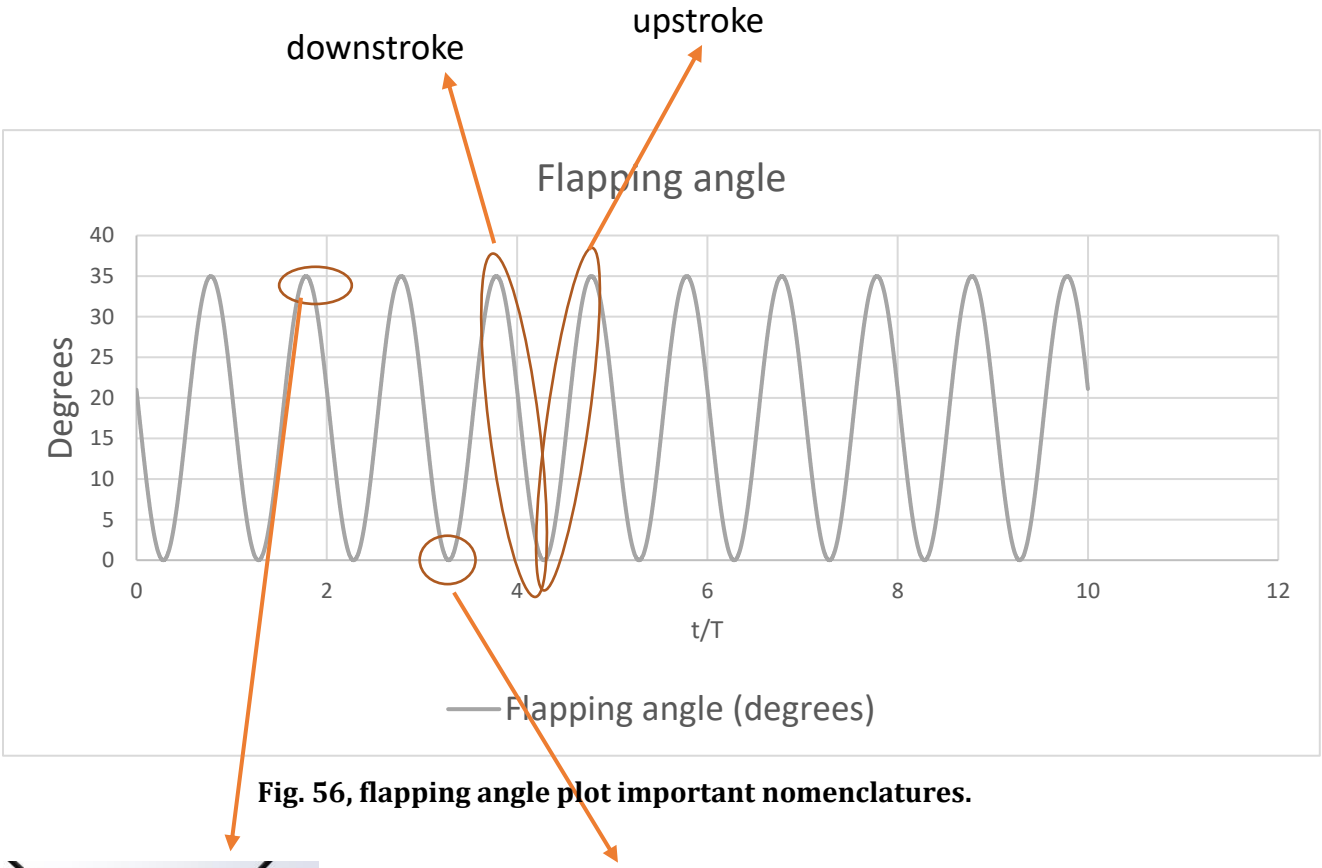

Fig. 56, flapping angle plot important nomenclatures.

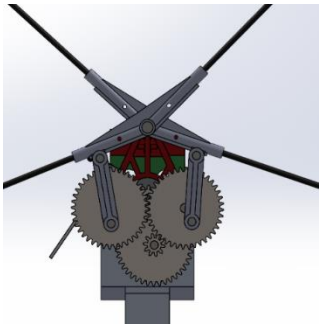

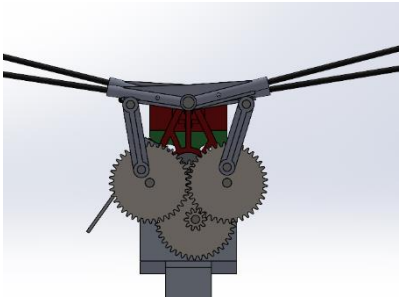

This naming will be very important for the coming discussions as it will be important to understand where the wing is at any instant.

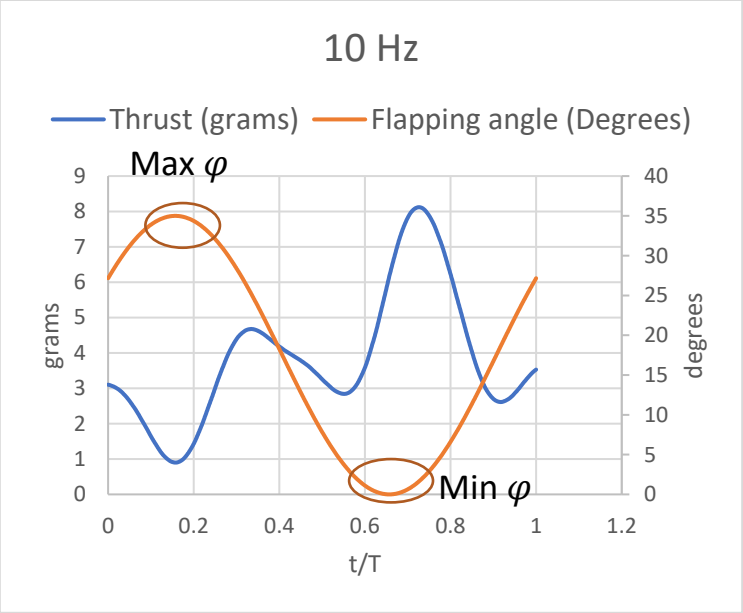

Fig. 57, thrust measurement with flapping angle Vs t/T at 10 Hz, stressing on max and min φ

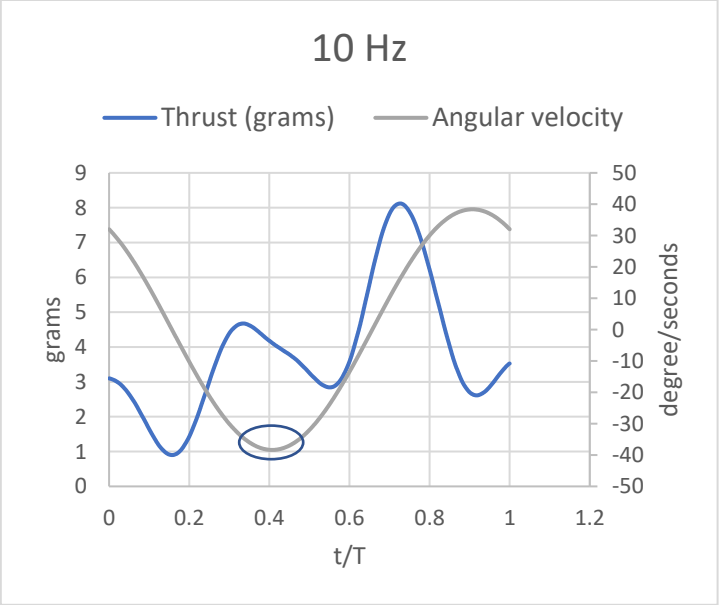

Fig. 58, thrust measurement with angular velocity Vs t/T at 10 Hz, stressing on maximum angular velocity

The flapping force per cycle, plotted with time is characterized by the existence of two peaks. As can be seen in the figures, the first peak is between the maximum and minimum flapping angles (circled in orange), with corresponds to the fact that the maximum angular velocity occurs somewhere in between as the wing is speeding up. This is confirmed by the presence of a negative peak in the Thrust Vs. angular velocity curve on the right (circled in blue). As mentioned before in this review and shown in [16], the leading-edge vortex is mainly characterized by a wing starting from zero to a maximum velocity at a high angle of attack, which is exactly the case here. This result is further confirmed by [32], in which the authors made a CFD simulation on an *Encarsia Formosa* wing and found that at very high speed in which the wings are approaching the clapping phase, there are two huge leading-edge vortices that are formed. The leading-edge vortices they found can be seen in figure (59).

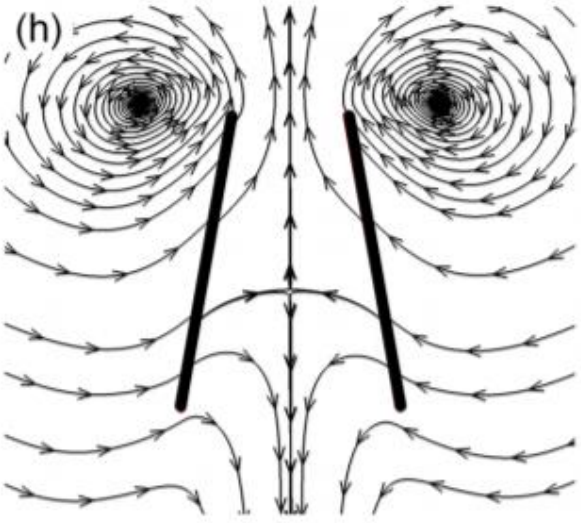

Fig. 59, taken from reference [32] large leading-edge vortices at high velocities

Going to the second peak, this peak is mostly dominated by the clapping effect. As can be seen in figure (60)

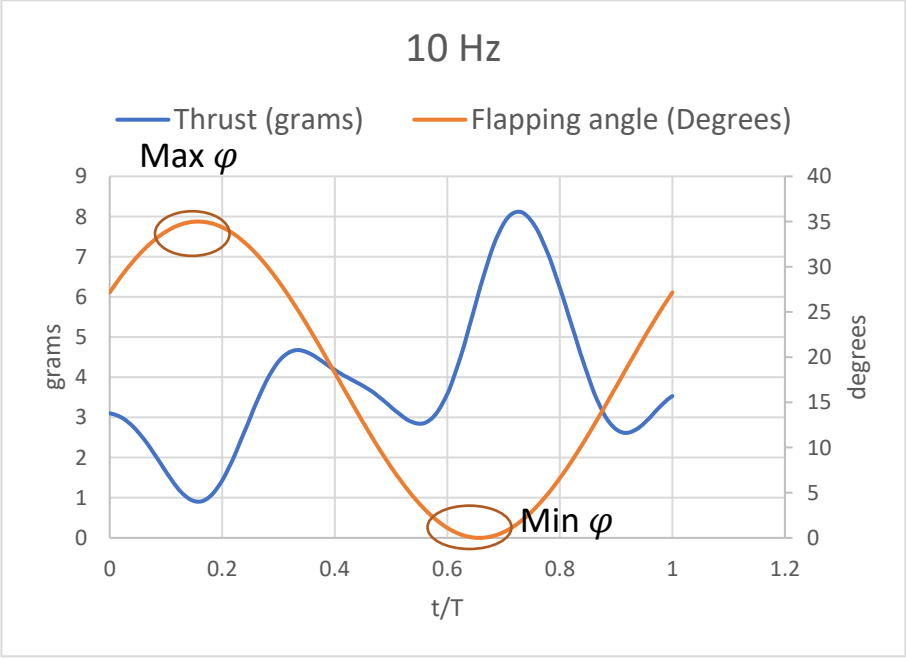

Fig. 60, thrust measurement with flapping angle Vs t/T at 10 Hz, 2nd peak position.

This peak happens right after the minimum flapping angle, in which the wings collide with each other. This is a direct of the flapping mechanism. This clapping squeezes the air

between the two wings, and thereby producing a jet flow that augments the thrust. The enhancement even surpasses the thrust coming from the LEV at the maximum speed phase, i.e., the first peak. One thing to note is that this squeezing actually increases in force as the frequency increases.

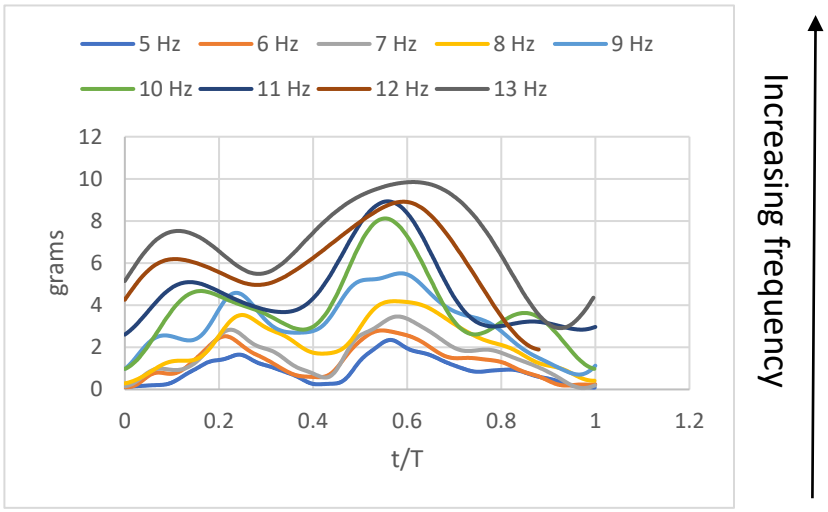

Fig. 61, the increase of the clapping effect with the increase in frequency

As can be seen in figure (61), as the frequency increases, the second peak rises more and more.

Another thing to note is that there is a time lag between the flapping angle in which the clapping should take effect, and the thrust peak at which it is seen. This lag is from the fact that the leading-edge "leads" the trailing edge during a cycle. The cause again is the wing flexibility. Remember, the magnet is placed on the rigid pard of the wing, which is a part of the rigid leading-edge. The material of the wing is a type of paper that is very thin, and thus it takes time for the full clap effect to be pronounced. This is shown in figure (). This lag

decreases as frequency increases. Going back to figures () and (), you can see that this lag is the largest at the 6 Hz measure, and minimal at the 12 Hz one.

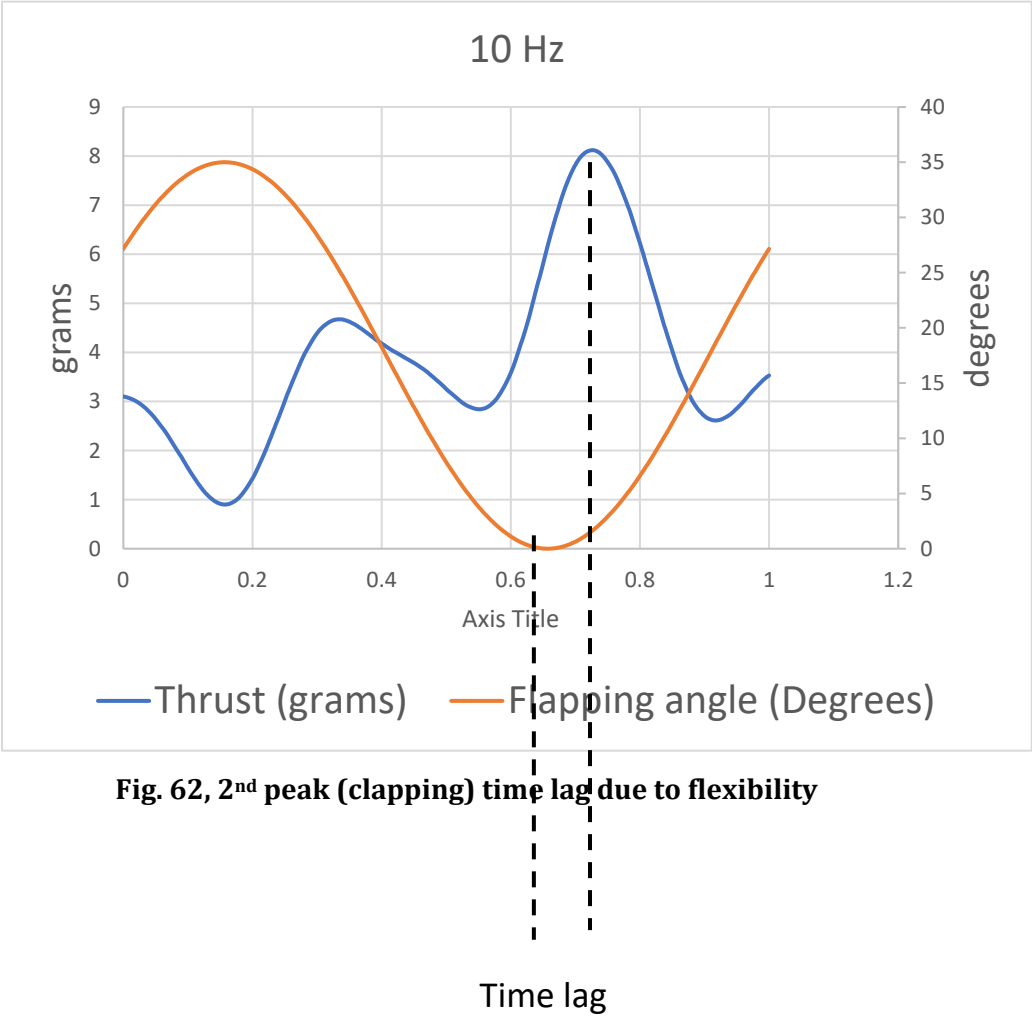

Fig. 62, 2nd peak (clapping) time lag due to flexibility

4.3.2 Efficiency

The performance curves will enable us to see the optimal design point that can will help us in designing the new Quad flapping drone here at the ADCL lab. Knowing these mentioned

details in the previous section, the thing missing is the optimum design point: which frequency and which wing area should we be operating around?

Using the same experimental setup, the thrust and lift output was averaged over a cycle for frequencies from 5-13 with an increment of 0.5 Hz. The same wing planform as in figure () was used (brought down here in figure ()), the only difference is that the half span was decreased. The large area half span is equals to 140 millimeters, while the small area half span is 95 millimeters. Since we are talking about an elliptic wing, this half span corresponds to the quarter ellipse semimajor axis.

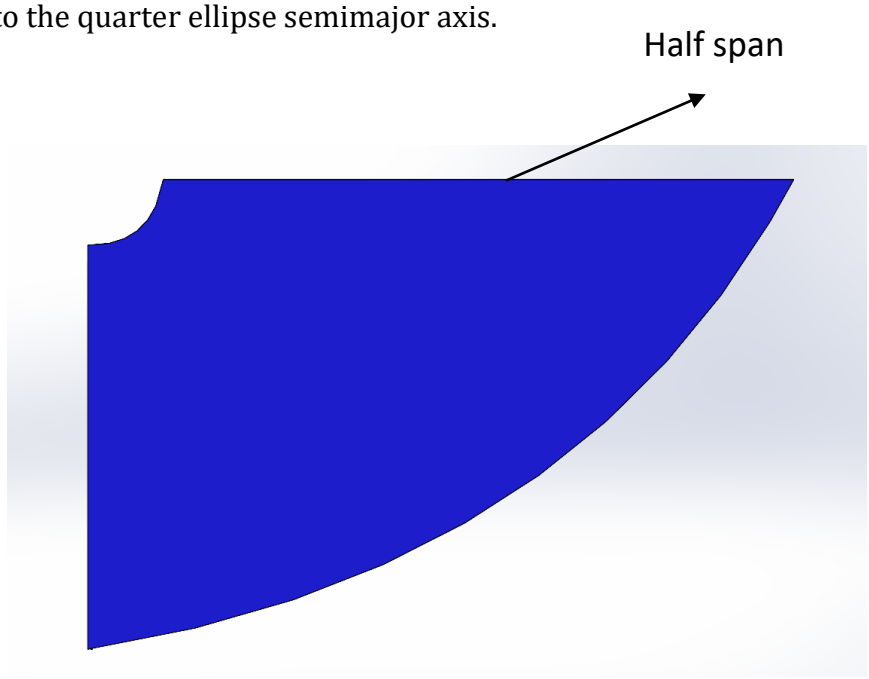

Fig. 63, elliptic wing planform

The ratio of the areas is:

$$- \quad \frac{Large\ area}{Small\ area} = 1.75 \qquad (48)$$

The average thrust and power per cycle were both nondimensionalized by:

- $C_T = \frac{Thrust}{0.5\rho V^2 S*4}$ (49)

- $C_P = \frac{Power}{0.5\rho V^3 S*4}$ (50)

In which the velocity here was taken to be the tip velocity at the leading edge. The velocity is calculated as:

- $V = 2\pi f * b * \varphi_{Max}$ (51)

where f is the flapping frequency, b is the semimajor axis or half span, φ_{Max} is the maximum flapping angle, which is taken constant equals to 35, and the constant of 4 is for having 4 wings. The results are shown in figures (65), (66), (67):

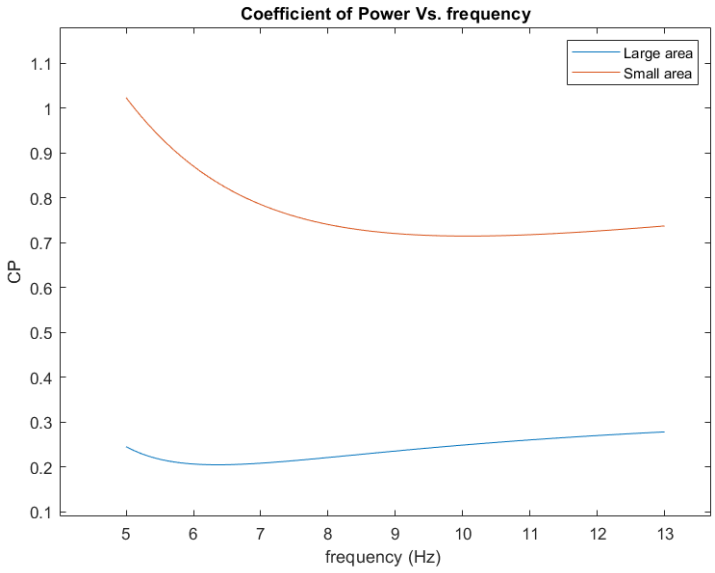

Fig. 64, coefficient of power with frequency for small and large areas

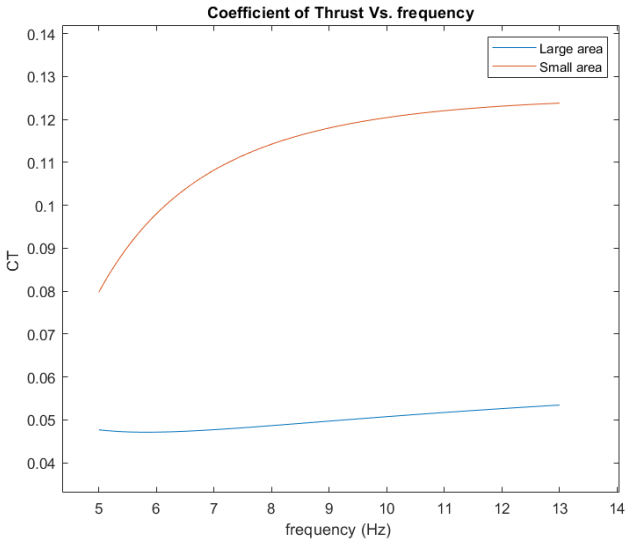

Fig. 65, coefficient of thrust with frequency small and large areas.

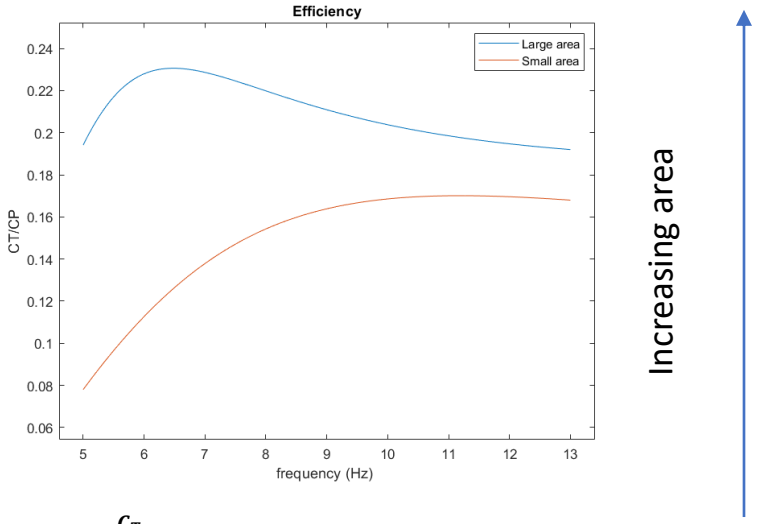

Fig. 66, $\frac{C_T}{C_P}$ (efficiency) curve for small and large areas

The efficiency curve is obtained by dividing the calculated coefficient of thrust by coefficient of power per cycle. As can be seen in figure (64), the C_T of the smaller area is higher than that of the larger one. It is logical in a mathematical sense, since the thrust is now divided by a smaller area. The same concept applies to the C_p also.

The result coming from the efficiency curve actually tells us that the increase in area is favorable, which is a very great thing to have. Increasing the area means increase thrust with a very minimal weight addition, which is always favorable. One reason for this trend that we see is that the wing flexibility used here may be optimized for big area. The smaller wing used here was made by cutting a part of the leading edge. It may be that smaller area might need similar optimization for maximum efficiency. A small thing to note is that the curve here is very smooth because fitting was used after the obtaining of thrust and power per cycle.

Another perspective for looking at the curve in figure (66), is that small insects always seem to be hovering at higher frequencies when compared to big flyers, in a way that is consistent with this curve. As can be seen, the curve is shifted to the left as the area increases.

A small note on the sizing of the bird. The size of the wing is an off-shelf one bought online. The setup was ready when I came to start to work, which is the big area one in figures (44-46). The smaller area one was cut by hand, that is why I mentioned the optimization note earlier.

Chapter 5

Conclusion and future work

5.1 Conclusion

Flapping wing aerodynamics was discussed for a four-winged flapping mechanism. This system was composed of the flapping mechanism and the four-axis load cell to measure different forces and moments. The hall effect sensor was utilized to measure the frequency and to estimate the flapping angle position with time. The placement of the Hall effect sensor was substantial in that it was used in favor of motion capture in order not to affect the sensory of the mass matrix, i.e., any dynamics or kinematics of the wings. By having such information about the flapping angle, the thrust force was investigated along the

flapping angle to see where the dominating aerodynamics and its causes are. It was found that the thrust force is characterized by two peaks, one peak is caused by the leading- edge vortex (delayed stall) that is in turn caused by the speeding of the wing from zero angle to the max flapping angle. The results showed that this corresponded to the point of maximum velocity. The second peak was the direct cause of the clapping effect. The clapping effect is basically the collision of the upper and lower wing at zero flapping angle. This collision yielded a jet of velocity which augmented the lift even higher beyond the first peak. To utilize such concepts to the use of FWMAV, performance curves were derived for two different areas. The larger area showed larger efficiency, this is favorable since this will produce large thrust with a small added weight. This can a way be revolutionary to flight in the sense of efficiency that less lift will be needed than the rigid wing one.

5.2 Future work

The next steps will be toward design, build a fly a quad flapping drone based on the aerodynamics that was just explained here in this work. The clapping mechanism is to be more utilized into making a double clapping flapper. The optimal design point coming from the efficiency curves would be used for preliminary design purposes.

Secondly, the efficiency curve showed a very favorable feature in the sense that it increases with the increase in area. This has to be investigated more and with more areas, especially in increasing the area trend. Because a legitimate question to be asked is that until what area can we increase? Can we go to full scale aircraft?

Lastly, in order to know the physics more, a PIV setup can be put in use. This will help in the seeing of the sizes and positions of the vortices.

Bibliography

1. Ellington, C. P. (1984a). The aerodynamics of hovering insect flight. I. The quasi-steady analysis. *Phil. Trans. R. Soc. Lond. B* **305**, 1–15.
2. Ellington, C. P**.** (1984b). The aerodynamics of hovering insect flight. II. Morphological parameters. *Phil. Trans. R. Soc. Lond. B* **305**, 17–40.
3. Ellington, C. P. (1984c). The aerodynamics of hovering insect flight. III. Kinematics. *Phil. Trans. R. Soc. Lond. B* **305**, 41–78.
4. Ellington, C. P. (1984d). The aerodynamics of hovering insect flight. IV. Aerodynamic mechanisms. *Phil. Trans. R. Soc. Lond. B* **305**, 79–113.
5. T. Theodorsen," General theory of aerodynamic instability and the mechanism of flutter," Tech. Rep. NACA-TR-496, National Advisory Committee for Aeronautics, Hampton, (1935).
6. H. Wagner, "Uber die Entstehung des dynamischen Auftriebes von Tragflugeln," Mathematica, vol. 5, pp. 17–35, (1925).
7. Weis-Fogh, T. & Jensen, M. (1956) Biology and physics of locust flight. I. Basic principles in insect flight. A critical review. *Phil. Trans. R. Soc. Lond.* B **239**, 415-458.

8. Weis-Fogh, T. (1956) Biology and physics of locust flight. II. Flight performance of the desert locust (Schistocerca *gregaria). Phil. Trans. R. Soc. Lond.* B **239**, 459-510.
9. Holst, E. v. & Kuchemann, D. (1942) Biological aerodynamical problems in animal flight. *J. R. Aero. Soc.* **46,** 39-56.
10. Walker, G. T. (1925) The flapping flight of birds. *J. R. Aero. Soc.* **29,** 590-594.
11. Walker, G. T. (1927) The flapping flight of birds. *J. R. Aero. Soc.* **31,** 337-342.
12. Osborne, M. F. M. (1951) Aerodynamics of flapping flight with applications to insects. *J. Exp. Biol.* **28,** 221-245.
13. Weis-Fogh, T. (1972). Energetics of hovering flight in hummingbirds and Drosophila. *J. exp. Biol*. **56**, 79-104.
14. Weis-Fogh, T. (1973) Quick estimates of flight fitness in hovering animals, including novel mechanisms for lift production. J. *exp. Biol.* **59,** 169- 230.
15. Maxworthy, T. (1979) Experiments on the Weis-Fogh mechanism of lift generation by insects in hovering flight. Part 1. Dynamics of the 'fling'. *J. Fluid Mech.* **93**, 47-63.
16. Dickinson, M. H., Lehmann, F.-O. and Sane, S. P**.** (1999). Wing rotation and the aerodynamic basis of insect flight. *Science* **284**, 1954–1960.
17. Ellington, C. P. (1984e). The aerodynamics of hovering insect flight. V. A vortex Theory. *Phil. Trans. R. Soc. Lond. B* **305**, 115–144.
18. Ellington, C. P. (1984f). The aerodynamics of hovering insect flight. VI. Lift and power requirements. *Phil. Trans. R. Soc. Lond. B* **305**, 145–181.
19. J. Marden, *J. Exp. Biol.* **130**, 235 (1987).
20. Ellington, C. P. (1980) Vortices and hovering flight. In Instationare Effecte an schwingenden Tierflugeln (ed. W. Nachtigall) pp. 64-101. Wiesbaden: Franz Steiner.

21. H. E. Taha, M. Kiani, T. L. Hedrick, J. S. M. Greeter, Vibrational control: A hidden stabilization mechanism in insect flight. *Sci Robot.* **5**, eabb1502 (2020).
22. Fung, Y. C. (1969). An Introduction to the Theory of Aeroelasticity. New York: Dover.
23. Taha, H. E., Hajj, M. R., & Beran, P. S. (2014). State-space representation of the unsteady aerodynamics of flapping flight. Aerospace Science and Technology, 34, 1-11.
24. M. Sun, G. Du, Lift and power requirements of hovering insect flight, Acta Mech. Sin. 19 (5) (2003) 458–469.
25. B. Van der Wall, J.G. Leishman, The influence of variable flow velocity on unsteady airfoil behavior, J. Am. Helicopter Soc. 39 (4) (1994).
26. Wang, Z. J., Birch, J. M., and Dickinson, M. H., "Unsteady Forces in Hovering Flight: Computation vs Experiments," Journal of Experimental Biology, Vol. 207, No. 3, 2004, pp. 449–460.
27. Sun, M., and Xiong, Y., "Dynamic Flight Stability of a Hovering Bumblebee," Journal of Experimental Biology, Vol. 208, No. 3, 2005, pp. 447–459
28. Sane, S. P., & Dickinson, M. H. (2002). The aerodynamic effects of wing rotation and a revised quasi-steady model of flapping flight. Journal of Experimental Biology, 205(8), 1087–1096.
29. Sun, M.,Wang, J., and Xiong,Y., "Dynamic Flight Stability of Hovering Insects," Acta Mechanica Sinica, Vol. 23, No. 3, 2007, pp. 231–246.
30. A. A. Agračev, R. V. Gamkrelidze, Exponential representation of flows and a chronological enumeration. Mat. Sb. 107, 467–532 (1978).

31. A. Sarychev, Stability criteria for time-periodic systems via high-order averaging techniques, in Nonlinear Control in the Year 2000, A. Isidori, F. Lamnabhi-Lagarrigue, W. Respondek, Eds., vol. 2 of Lecture Notes in Control and Information Sciences (Springer-Verlag, 2001), pp. 365–377.
32. Cheng, Sun, Revisiting the clap-and-fling mechanism in small wasp Encarsia formosa using quantitative measurements of the wing motion. Phys. Fluids 31, 101903 (2019)
33. Percin, Hu, Ouedheusden, Remes, Scarano, Proceedings of the International Micro Air Vehicles conference (2011)
34. Taha, H. E., Hajj, M. R., & Nayfeh, A. H. (2014). Longitudinal Flight Dynamics of Hovering MAVs/Insects. Journal of Guidance, Control, and Dynamics, 37(3), 970–979.
35. Taha, H. E and A. Rezaei, "On the Dynamics of Unsteady Lift and Circulation and the Circulatory-Non-circulatory Classification," Jan 2019.
36. Taha, H., & Rezaei, A. S. (2019). Viscous extension of potential-flow unsteady aerodynamics: the lift frequency response problem. Journal of Fluid Mechanics, 868, 141–175. https://doi.org/10.1017/jfm.2019.159
37. Taha, H. E., & Rezaei, A. S. (2021, January). State Space Modeling of Viscous Unsteady Aerodynamic Loads. AIAA Scitech 2021 Forum. https://doi.org/10.2514/6.2021-1830
38. Taha, H. E., & Rezaei, A. S. (2018, January). Unsteady Viscous Lift Frequency Response Using The Triple Deck Theory. 2018 AIAA Aerospace Sciences Meeting. https://doi.org/10.2514/6.2018-0038

39. Hassan, A. M., & Taha, H. E. (2018). Differential-Geometric-Control Formulation of Flapping Flight Multi-body Dynamics. Journal of Nonlinear Science, 29(4), 1379–1417. https://doi.org/10.1007/s00332-018-9520-8

40. Taha, H. E., Tahmasian, S., Woolsey, C. A., Nayfeh, A. H., & Hajj, M. R. (2015). The need for higher-order averaging in the stability analysis of hovering, flapping-wing flight. Bioinspiration & Biomimetics, 10(1), 016002. https://doi.org/10.1088/1748-3190/10/1/016002

41. Taha, H., Kiani, M., & Navarro, J. (2018). Experimental Demonstration of the Vibrational Stabilization Phenomenon in Bio-Inspired Flying Robots. IEEE Robotics and Automation Letters, 3(2), 643–647. https://doi.org/10.1109/lra.2017.2778759

42. Fouda, M., & Taha, H. E. (2021, January). Experimental Investigations of Airplane Maneuverability and Stability in Stall. AIAA Scitech 2021 Forum. https://doi.org/10.2514/6.2021-1819